

Chapter – IV

Effect of 120 MeV Ni¹⁰⁺ Ions Irradiation on Polymer Composites

Abstract

In this chapter swift heavy ion (120MeV, Ni¹⁰⁺ ions) induced modification of Ferric oxalate/Pd(acac)/Ni powder dispersed PMMA films at the fluences of 1×10^{11} and 5×10^{12} ions/cm² were studied. SHI induces more pronounced effect on the physico-chemical properties of the composites compared to proton irradiation. Significant improvement has been observed in dielectric and mechanical properties after Ni¹⁰⁺ ion irradiation. XRD analysis reveals the decrease in crystalline size and % crystallinity after SHI irradiation. AFM result shows that average surface roughness increases after irradiation. It might be due to large sputtering effect on the surface due to SHI. SEM images of PMMA+Fo shows blister formation on the surface after irradiation. Images of PMMA+Ni illustrate considerable damage on the surface. This damage is responsible for amorphization of composite structure which is corroborated with XRD results.

4.0 Introduction

When SHI interact with matter, energy is transferred to the medium and this energy absorption leads to electrical, mechanical, chemical and structural modification of the material. Interaction of high energy ion beam with polymer results in the formation of gaseous products accompanied by polymer crosslinking (i.e. formation of intermolecular bonds) [1], degradation (i.e. scission of bonds in the main polymer chain and inside chains) [2] and some other secondary processes [3]. Although both electronic and nuclear energy transfer can induce crosslinking as well as scission as would be intuitively expected, experimental evidence suggests that electronic stopping causes more crosslinking while nuclear stopping causes more scissions [4]. However in case of SHI irradiation, electronic energy loss is more prominent.

Ion irradiation of polymeric materials is followed by the processes of macromolecular destruction, cross-linking, free radicals formation, carbonization and oxidation [5, 6]. Therefore, the understanding of certain structural rearrangement influence on the suitable electrical, optical etc. properties of the polymeric materials/composites opens a way to design devices with required parameters.

So far not much work have been reported which deals with the SHI effect on composites. The aim for this work is to produce composites with high dielectric constants and low loss tangent which is the requirement of telecommunications industry, microelectronics, EMI shielding, etc. where radiative environment exists.

For that purpose, we synthesized following polymer composites and studied the effect of 120 MeV Ni¹⁰⁺ ions on them,

- (i) PMMA+Fo [7]
- (ii) PMMA+Pd(acac) [8]
- (iii) PMMA+Ni [9]

(iv) PI+Fe [10]

Properties and preparation method of composites have been discussed in Chapter-2. The chapter also explain the importance and method of thin film deposition. Fe dispersed PI films were prepared on Glass and Silicon substrate by RF co-sputtering. All films were irradiated with 120 MeV Ni¹⁰⁺ ions at the fluences of 1x10¹¹ and 5x10¹² ions/cm² using Pelletron accelerator at Inter University Accelerator Centre (IUAC), New Delhi. Magnetic properties and surface morphology of pristine and irradiated thin films were studied. AC electrical, mechanical, structural, chemical properties and surface morphology of the other composites were carried out.

4.1 Effect of SHI (120 MeV Ni¹⁰⁺ ions) on PMMA+Fe composites

4.1.1 AC electrical properties

(i) AC electrical Conductivity

The AC conductivity of the pristine and irradiated composite films was calculated using equation 2.3.13 (Section 2.3 of Chapter-2). Figure 4.1 (a-d) shows the conductivity as a function of the frequency and fluence. Dependence of conductivity on filler concentration at fixed frequency of 1 MHz is also shown in Fig. 4.1(e).

The AC conductivity of the composites increases with increasing frequency and also with concentration of filler. It is assumed that an electrical conducting path and network of connections could be formed in the composites with increasing the content of filler. It is known that electrical conductivity of such composites depends on the type and concentration of the filler [11, 12]. It is also observed that the conductivity increases on increasing ion beam fluence (Fig. 4.1).

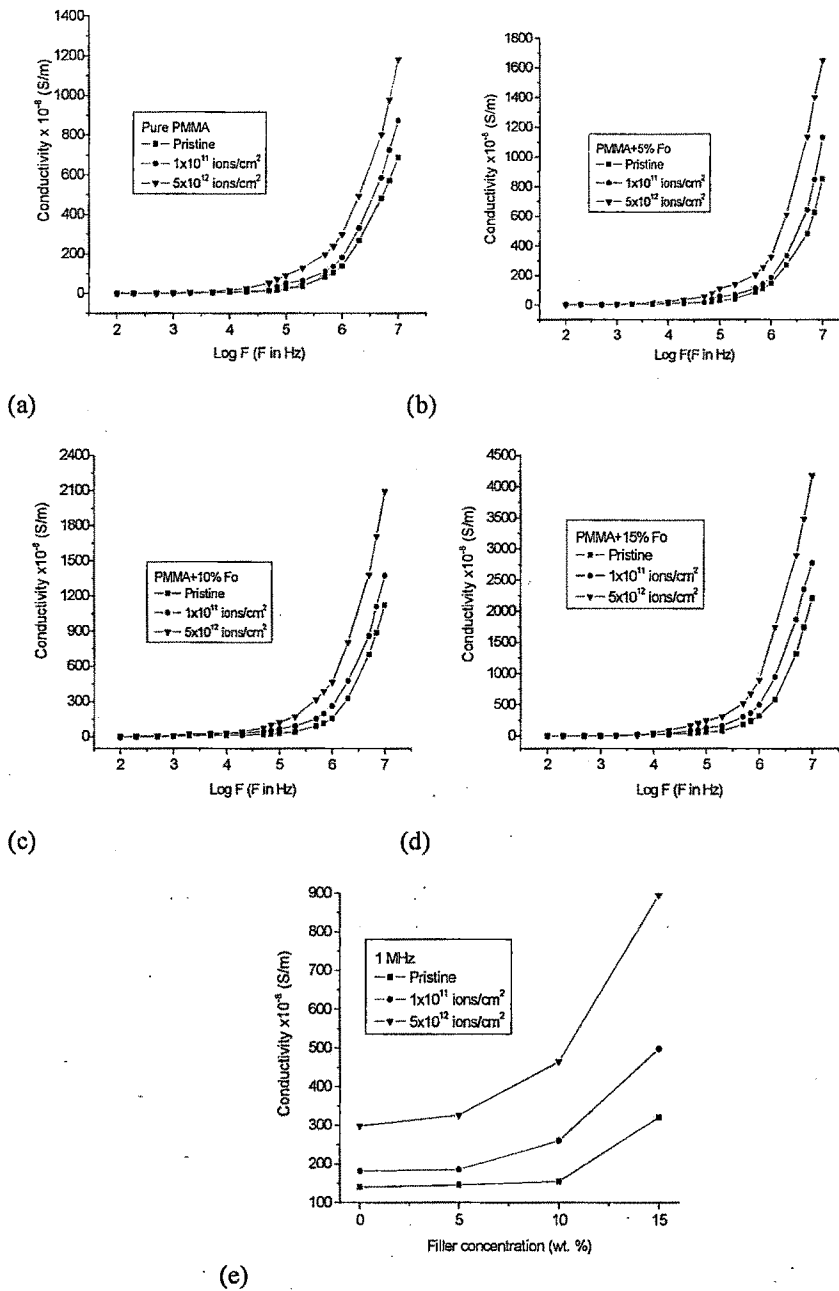


Fig. 4.1 AC conductivity versus log frequency of pristine and irradiated films of (a) Pure PMMA, (b) PMMA+5%Fo, (c) PMMA+10%Fo and (d) PMMA+15%Fo (e) Variation of AC conductivity with filler concentration at 1 MHz

Irradiation is expected to promote the metal to polymer bonding and convert the polymeric structure into a hydrogen depleted carbon network due to emission of hydrogen and/or other volatile gases. This carbon network is believed to make the polymers more conductive [7, 13-15].

(ii) Dielectric property

Dielectric constant of all samples was determined using equation 2.3.15 as discussed in Chapter-2. Fig. 4.2(a-d) shows the variation of dielectric constant of pristine and irradiated PMMA/Fo composites as a function of frequency and fluence. For pristine and irradiated composite films at all concentrations, the dielectric constant remains almost constant up to 100 kHz. At these frequencies, the motion of the free charge carriers is constant and so the dielectric constant presumably remains unchanged. As frequency increases further (i.e. beyond 100 kHz), the charge carriers migrate through the dielectric and get trapped against a defect sites and induced an opposite charge in its vicinity. At these frequencies, the polarization of trapped and bound charges cannot take place and hence the dielectric constant decreases [19, 20]. The dielectric constant decreases at higher frequencies (i.e. beyond 100 kHz) obeys the Universal law [21] of dielectric, i.e. $\epsilon \propto f^{-n}$, where n is the power law exponent and varies between zero to one. It is observed that n decreases as concentration increases and increases as fluence increases. In the present case n varies between 0.7 and 0.91. Fig.4.2 clearly shows that the frequency dependence of dielectric constant, ϵ , obeys Universal law at higher frequencies. The variation of dielectric constant as a function of filler concentration at different fluences for fixed frequency of 1 MHz is shown in Fig 4.2(e). A moderate increase in dielectric constant is observed for irradiated films at a fluence of 1×10^{11} ions/cm² whereas a significant change has been observed at a fluence of 5×10^{12} ions/cm².

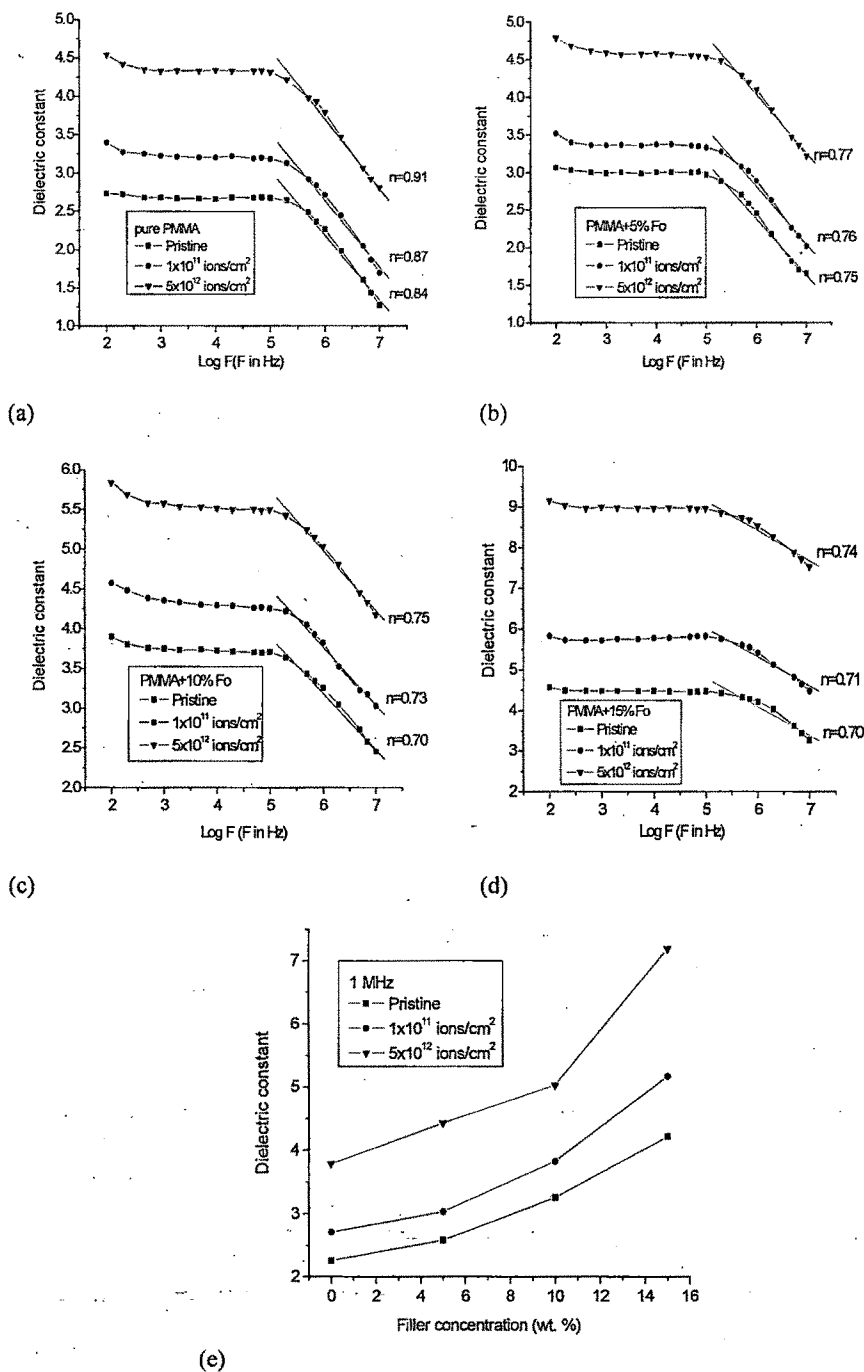


Fig. 4.2 Dielectric constant versus log frequency for pristine and irradiated films of (a) Pure PMMA, (b) PMMA+5%Fo, (c) PMMA+10%Fo and (d) PMMA+15%Fo composite (e) Dielectric constant versus filler concentration at 1 MHz

The increase in the dielectric constant with filler content is a direct consequence of interfacial polarization effect between polymer and the filler particles [19]. The quantity of the accumulated charges will increase in the composite after doping because of the polarization of the PMMA/filler at the interfaces. The polarization makes an additional contribution to the charge quantity.

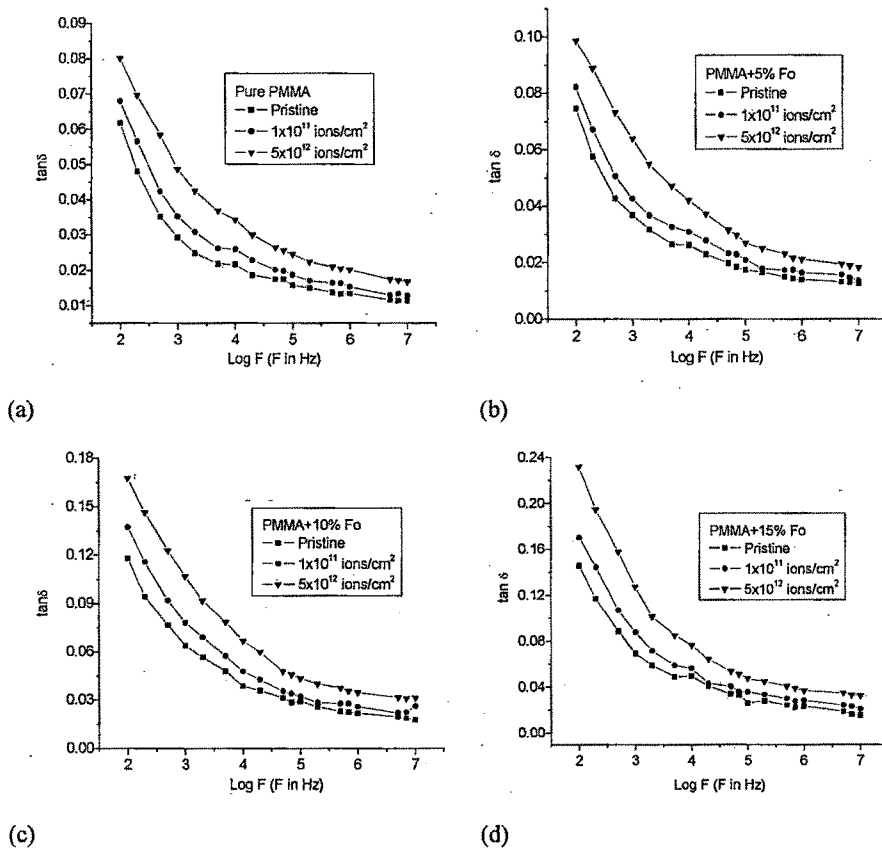


Fig. 4.3 Dielectric loss versus log frequency for pristine and irradiated films of (a) Pure PMMA, (b) PMMA+5%Fo, (c) PMMA+10%Fo and (d) PMMA+15%Fo composite

From this point of view the dielectric constant of the composites will be higher than that of the pure polymer and it increases with increasing the filler content [20, 21]. The experimental results in Fig. 4.2 also support this explanation. Therefore, the materials with high dielectric constant could be prepared by adding the conducting

fillers. The dielectric constant increases as fluence increases. The observed nature of the fluence dependence of dielectric constant in a studied frequency range can be explained by the prevailing influence of the enhanced free radicals, unsaturations etc. due to the irradiation [22].

Fig. 4.3 (a-d) shows the frequency dependence of the dielectric loss of the composite at different fluences. The dielectric loss decreases exponentially and then became less dependent on frequency. This is because the induced charges gradually fail to follow the reversing field causing a reduction in the electronic oscillations as the frequency is increased. The increase in dielectric loss with increasing filler contents may be attributed to the interfacial polarization mechanism of the heterogeneous system. Further, moderate increase in $\tan\delta$ occurs due to the irradiation [23-25].

4.1.2 Microhardness

The Vickers' hardness number (H_v) was determined with Vickers microhardness tester consisting of Vickers diamond pyramidal indenter having a square base and 136° pyramidal angle of Future Tech. FM-700, Japan.

The H_v value was calculated using the following equation 2.3.16 as discussed in section 2.3.2 of Chapter-2.

$$H_v = 1.8544 \times \frac{P}{d^2}$$

where P is the indenter load in mN obtained as the product of the load (in g) and gravitational acceleration (g) = 9.8 ms^{-2} , d is the average of the two diagonal lengths in microns.

Fig. 4.4 (a-d) shows the plots of the Vickers microhardness (H_v) versus applied load (P) at different concentration of filler for unirradiated and irradiated samples.

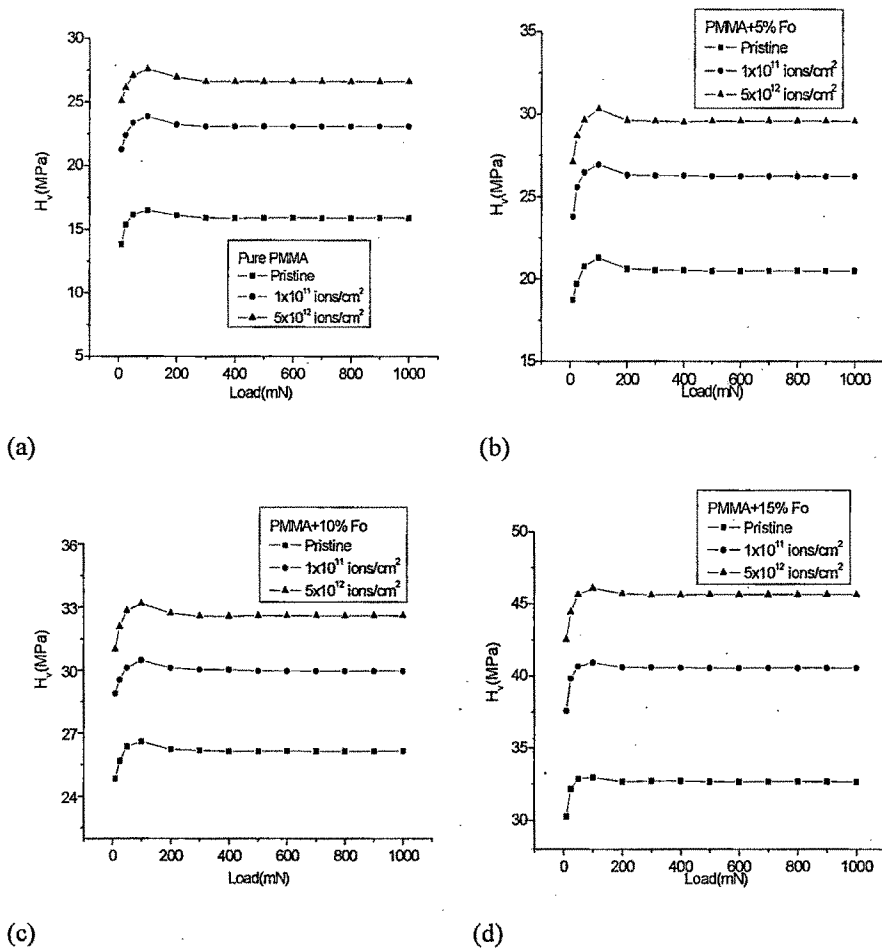


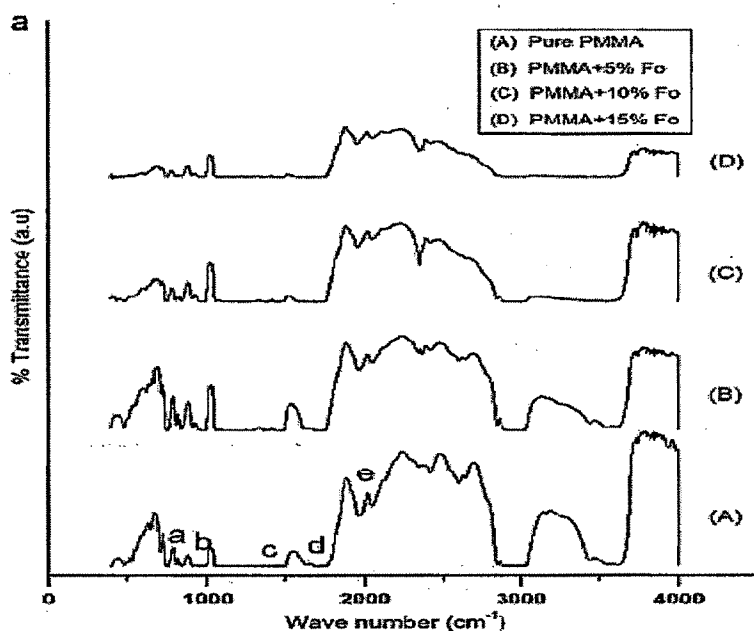
Fig. 4.4 Vickers microhardness versus applied load for pristine and irradiated films of (a) Pure PMMA, (b) PMMA+5% Fo, (c) PMMA+10% Fo and (d) PMMA+15% Fo

It is evident that H_v value increases with the load upto 100 mN and then decreases and became saturated beyond a load of 300 mN. On applying the load, the polymer is subjected to some strain hardening. Finally when H_v value tends to become constant the polymer is completely strain hardened. The value obtained from the saturation region, therefore, represents the true hardness of the bulk material, since at high loads the indenter penetration depth is also high and surface effects become insignificant [4]. It is found that hardness increases as ferric oxalate concentration increases. This

may be due to the improvement in bonding properties. The hardness also increases as fluence increases. This may be attributed to the growth of a hydrogen depleted carbon network, which makes the polymer harder [4, 13].

4.1.3 FTIR analysis

Figure 4.5(a,b) show the FTIR spectra of the pristine and irradiated (at fluence of 5×10^{12} ions/cm²) samples at different concentrations, respectively. The presence of different functional groups in the structure has been identified as (a) 750 and 810 cm⁻¹; CH₂ rocking vibration (b) 700-1500 cm⁻¹; C-O stretching vibration (c) 1350-1450 cm⁻¹; C-H bending vibration (d) 1730 cm⁻¹; C=O stretching vibrations in the pendant group (-COOCH₃) of PMMA (e) 2010 cm⁻¹; C=C stretching vibration [26].



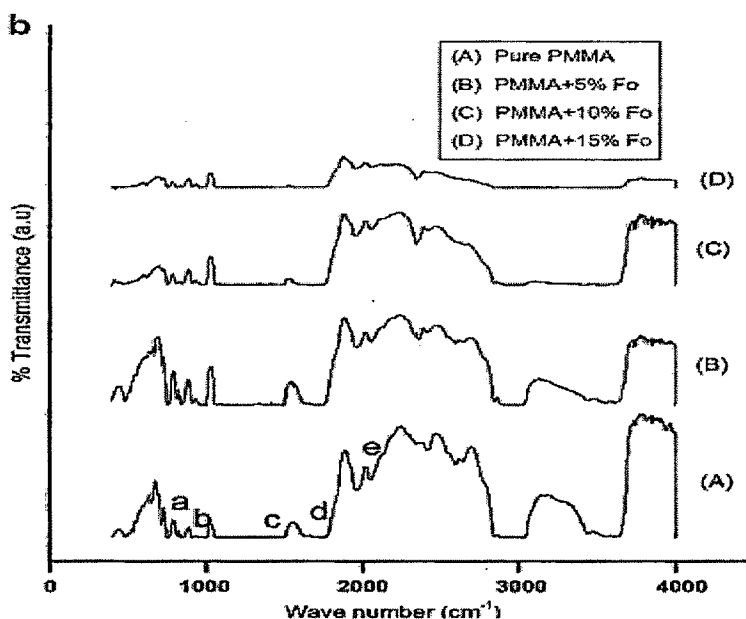


Fig. 4.5 FTIR spectra of (a) pristine and (b) irradiated (5×10^{12} ions/cm²) films

It is observed that intensity of functional groups decreases as filler concentration increases. These peaks decrease further also with the fluence. This shows that the C-O, C=O bonds and CH₂, CH₃ groups diminish with irradiation. It suggests the formation of carbon network due to the emission of hydrogen and/or other volatile gases.

4.1.4 Atomic force microscopy (AFM)

The surface morphology of pristine and irradiated films of pure PMMA and 5%, 10% and 15% Fo dispersed PMMA was studied by AFM on $2 \times 2 \mu\text{m}^2$ area as shown in Fig. 4.1.6 (a-h). Each AFM image was analyzed in terms of surface average roughness (Ra). The average roughness values obtained are 2.3, 4.7, 7.7 and 24.1 nm for pure PMMA and 5, 10 and 15% Fo dispersed PMMA samples respectively before irradiation. The roughness values of correspondingly irradiated (at a fluence of 5×10^{12} ions/cm²) samples are 4.8, 11.0, 19.5 and 33.4 nm respectively.

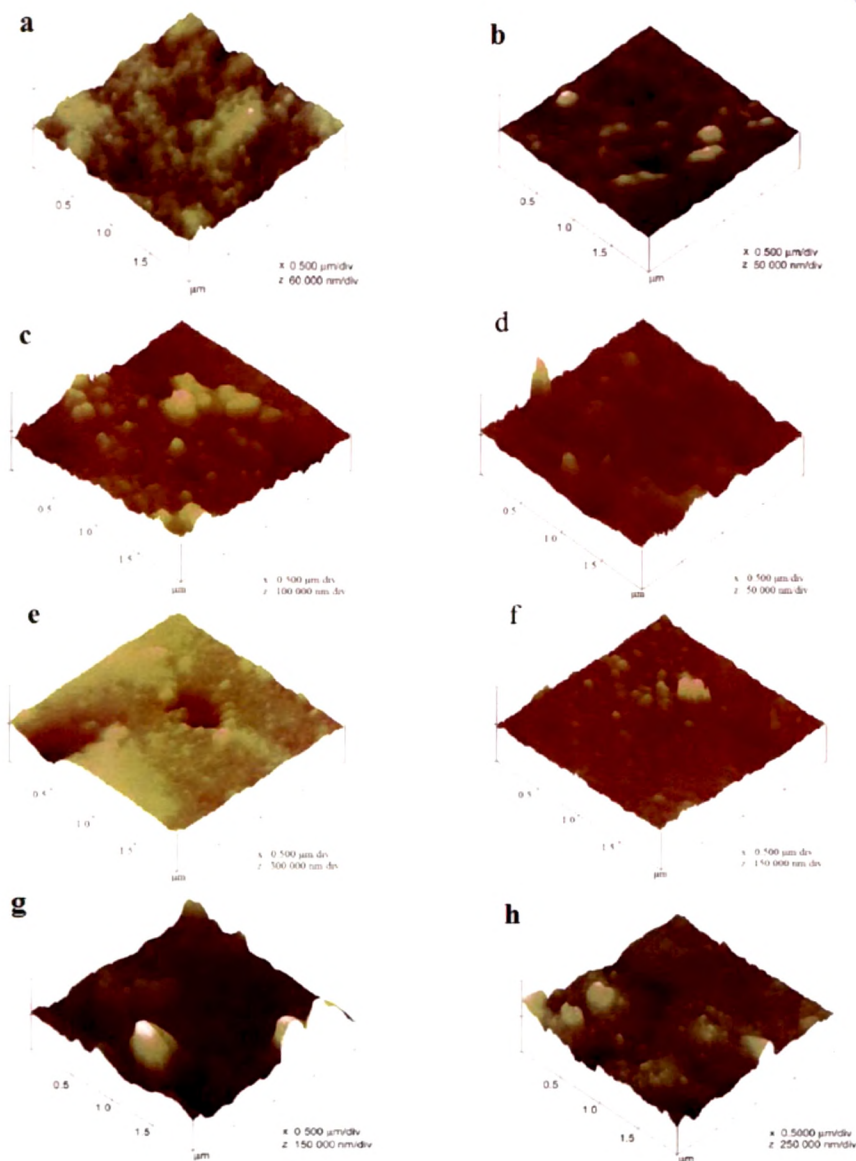


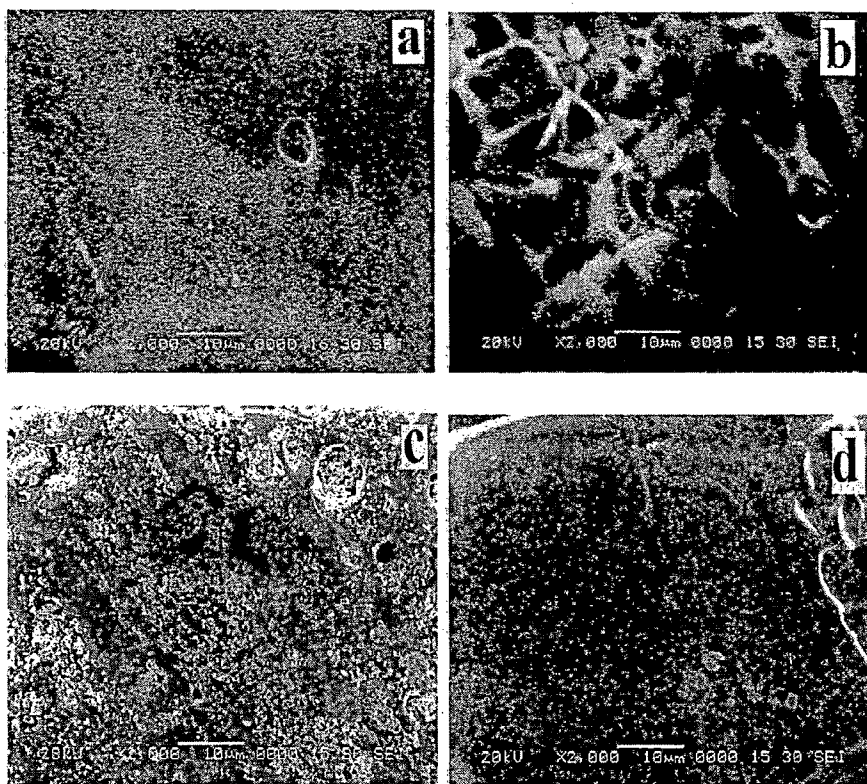
Fig. 4.6 AFM images of (a) Pure PMMA(pristine) (b) Pure PMMA(irradiated) (c) PMMA+5% Fo (pristine) (d) PMMA+5% Fo (irradiated) (e) PMMA+10% Fo (pristine) (f)PMMA+10% Fo (irradiated) (g) PMMA+15% Fo (pristine) (h) PMMA+15% Fo (irradiated) films

It is found that roughness increases as ferric oxalate concentration increases. The increase in roughness may be due to the increase of density and size of metal particles on the surfaces of the PMMA films [27]. Ion irradiation of polymers leads, in

general; to an increase in surface roughness due to large sputtering effects, which is also corroborated with SEM results.

4.1.5 Scanning electron microscopy

Fig. 4.7(a-h) shows the SEM images of pure PMMA and 5%, 10% and 15% ferric oxalate dispersed pristine and irradiated (5×10^{12} ions/cm²) composite films at 2000x magnification. After irradiation, blisters type of phenomenon could be seen on the surface of composites as obtained from SEM micrographs in Fig 4.7 (d,f,h).



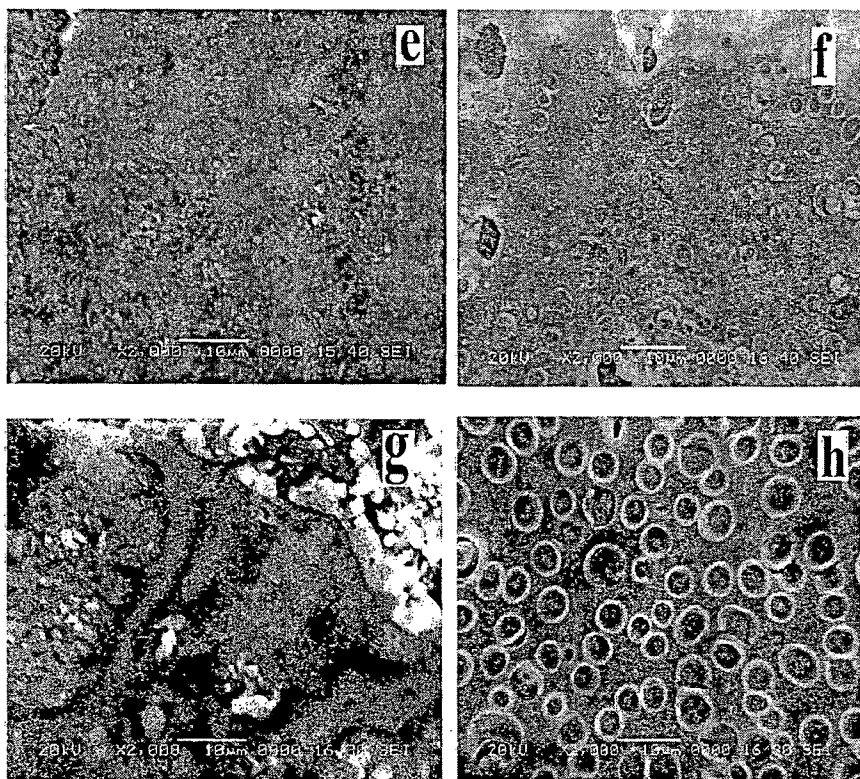


Fig. 4.7 SEM micrographs of (a) Pure PMMA(pristine), (b) Pure PMMA (irradiated), (c) PMMA+5%Fo (pristine), (d) PMMA+5%Fo (irradiated), (e) PMMA+10%Fo (pristine), (f) PMMA+10%Fo (irradiated), (g) PMMA+15%Fo (pristine) and (h) PMMA+15%Fo (irradiated) films

4.1.6 DSC analysis

Fig. 4.8 shows DSC thermograms of pristine PMMA, pristine and irradiated (5×10^{12} ions/cm²) PMMA+15%Fo samples. The results reveal that the glass transition temperature (T_g) increases for the composite as compared to pure PMMA. The increase in T_g of composites may be due to the interactions of ferric oxalate and PMMA in more ordered state [27]. After irradiation T_g decreases, which reveals the amorphization of the composite after irradiation.

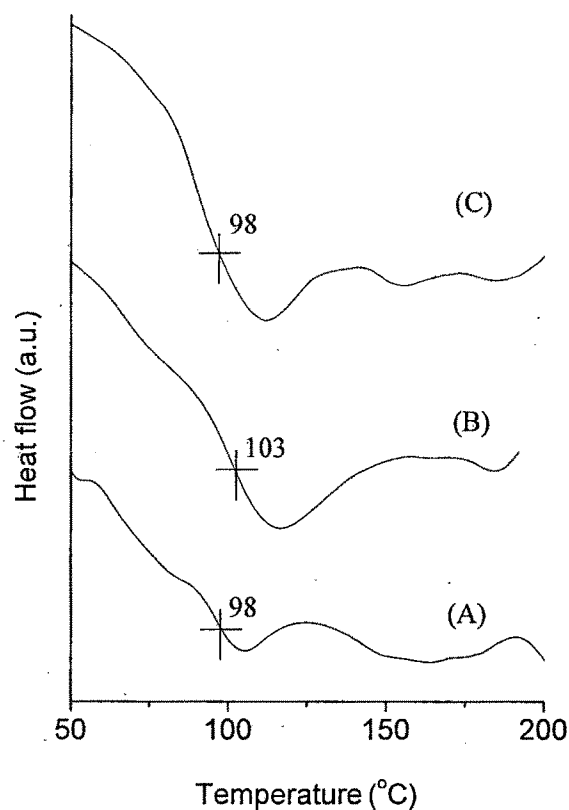


Fig. 4.8 DSC thermograms of (A) Pure PMMA(pristine), (B) PMMA+15%Fo (pristine) and (C) PMMA+15%Fo (Irradiated)

4.1.7 Conclusions

AC electrical properties and microhardness of pristine and irradiated organometallic compound dispersed PMMA films were investigated. The conductivity of the composites increases with an increase in the frequency, filler and also with ion fluence. Ion irradiation has shown significant enhancement in dielectric properties of the composites. The dielectric constant remains constant up to 100 kHz and then decreases slowly with increasing frequency and increases gradually with the increase of the concentration of filler. Dielectric loss/constant is observed to change significantly due to the irradiation. This might be attributed to breakage of chemical

bonds and resulting in the increase of free radicals, unsaturation, etc. The Vickers' microhardness of the composites increases by doping filler in polymer and also with the ion fluence. It may be due to (i) metal to polymer bonding and (ii) conversion of the polymeric structure in to hydrogen depleted carbon network due to the emission of hydrogen and/or other volatile gases. Thus irradiation makes the polymer more conductive and harder. FTIR results also reveal that there is decrease in peak intensity of few bonds due to the emission of hydrogen and other volatile gases upon irradiation. The surface roughness increases as ferric oxalate concentration increases and also with the fluence as observed from AFM studies. After irradiation, blisters type of phenomenon was observed in the micrographs of PMMA+Fo composites as revealed from SEM studies. DSC analysis reveals that the glass transition is affected by both – presence of filler and irradiation.

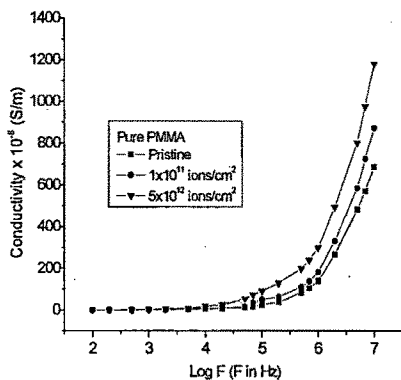
4.2 Effect of SHI (120 MeV Ni¹⁰⁺) on PMMA+Pd(acac) composites

4.2.1 AC electrical properties

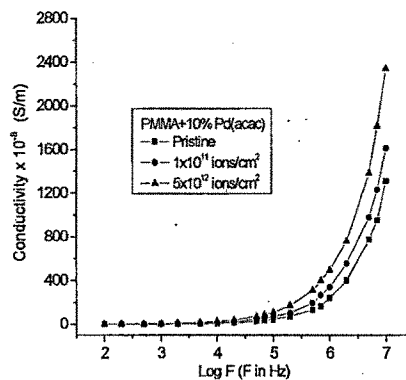
(i) AC electrical Conductivity

AC electrical conductivity was calculated using equation 2.3.13 (section 2.3.1) of Chapter-2. Figure 4.9(a-d) shows the variation of conductivity with frequency of applied field, filler concentration and fluence of ion beam. It was observed that conductivity increases with increasing concentration of dispersed Pd(acac) as well as with fluence.

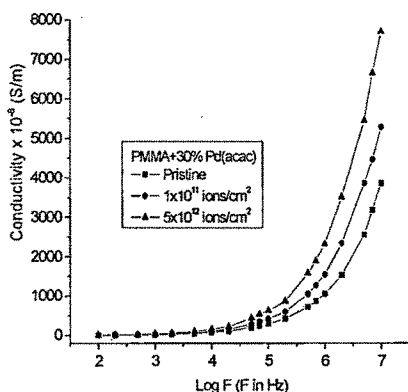
It is known that electrical conductivity of such composites depends on the type and concentration of the dispersed compound. The conductivity further increases after irradiation. Irradiation is expected to promote the metal to polymer adhesion and convert the polymeric structure into a hydrogen depleted carbon network. It is this carbon network that is believed to make the polymer more conductive [13].



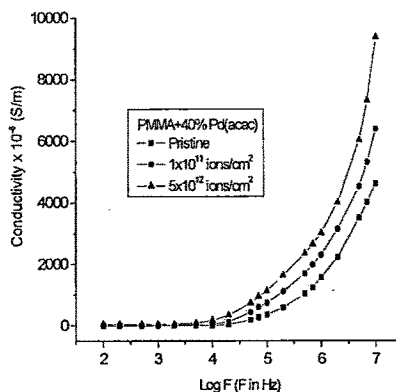
(a)



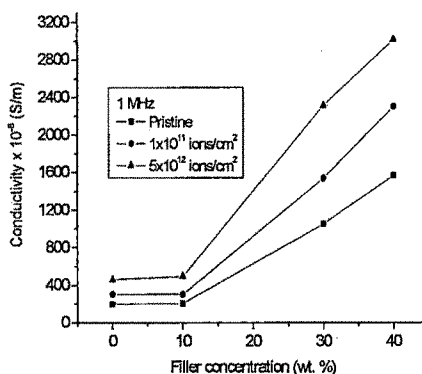
(b)



(c)



(d)



(e)

Fig. 4.9 AC conductivity versus log frequency for pristine and irradiated films of (a) Pure PMMA, (b) PMMA+10% Pd(acac) (c) PMMA+30% Pd(acac) (d) PMMA+40% Pd(acac) (e) AC conductivity versus filler concentration at 1 MHz frequency

Fig. 4.9(e) shows that conductivity increases with increasing filler concentration. Sudden increase in conductivity at 30% Pd(acac) dispersed composite indicates percolative behavior of the samples. This might be attributed to the conductive phase formed by dispersed organometallic compound in polymer matrix. As a result the conductivity of dispersed films increases on increasing the concentration of metallic compound in polymer matrix.

(ii) Dielectric property

Dielectric constant was calculated using equation 2.3.15 as explained in Chapter-2. Figure 4.10(a-d) shows the variation in dielectric constant with log frequency. It is observed that dielectric constant remains almost constant up to 100 kHz, because the motion of charge carriers is almost constant at these frequencies. Beyond this frequency, the dielectric constant decreases. As the frequency increases, the charge carriers migrate through the dielectric and get trapped against a defect sites and they induced an opposite charge in its vicinity, as a result, motion of charge carriers is slowed down and the value of dielectric constant decreases. The decrease in dielectric constant at higher frequency can be explained by Jonscher's power law i.e. $\epsilon \propto f^{n-1}$ where $0 < n < 1$ [18].

Due to dispersion of organometallic compound, the quantity of the accumulated charges will increase because of the polarization of the polymer/metal at interfaces. The polarization makes an additional contribution to the charge quantity. From this point of view, the dielectric constant of the composites will be higher than the pure polymer [21]. Our experimental results also support this explanation.

According to Dissado and Hill theory [29] at high frequency, intra-cluster motions are dominant. In intra-cluster motions, the relaxation of a dipole will produce a 'chain' response in its neighbouring dipoles and the reaction of the neighbouring dipoles will, in turn, affect the first dipole, so the overall effect will be seen as a single cluster dipole moment relaxation [28]. This reduces the dielectric constant at these frequencies. It is also observed that the dielectric constant increases on increasing the concentration of filler as shown in Fig. 4.10 (e).

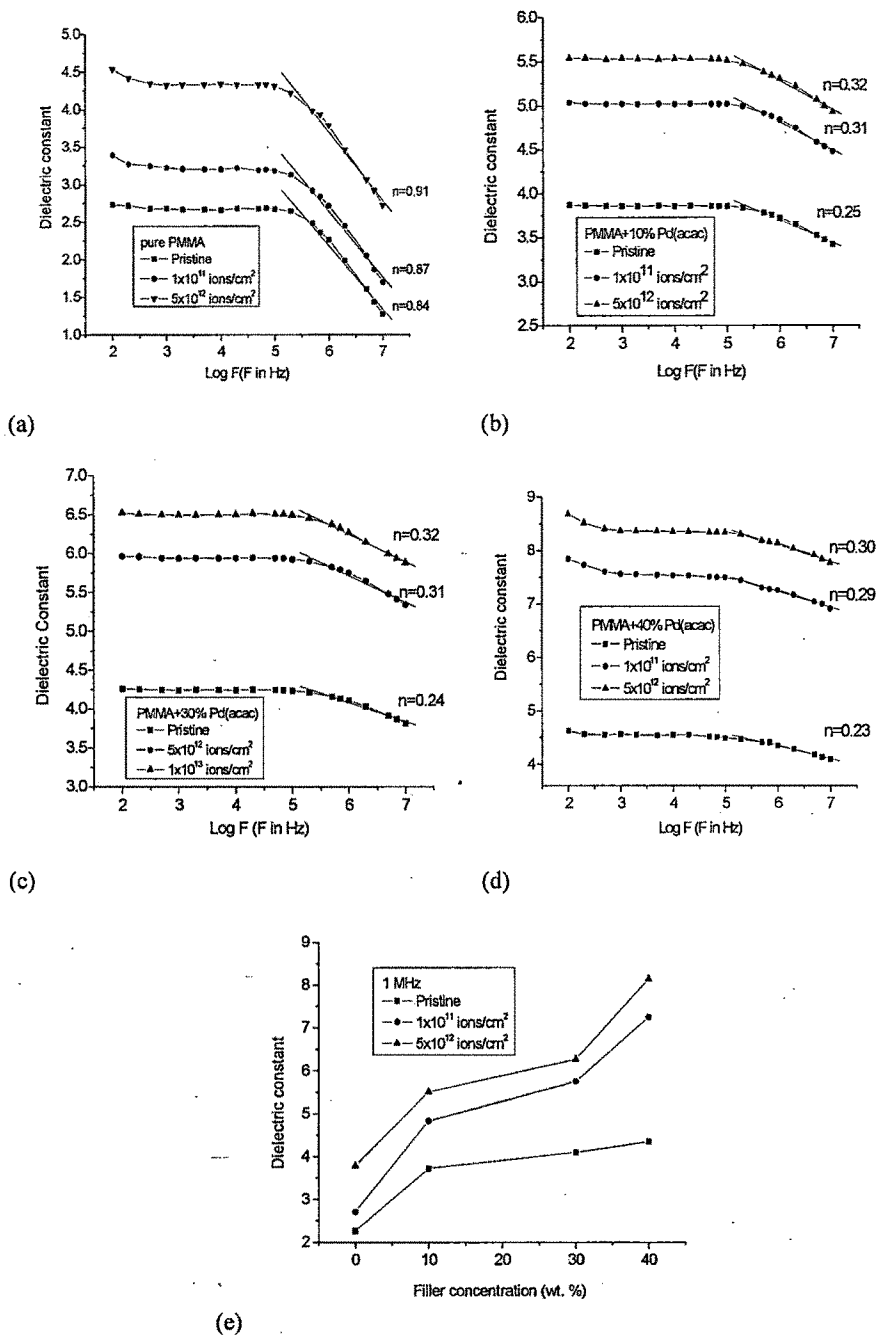


Fig. 4.10 Dielectric constant versus log frequency of pristine and irradiated films of (a) Pure PMMA, (b) PMMA+10% Pd(acac), (c) PMMA+30% Pd(acac), (d) PMMA+40% Pd(acac) films (e) Dielectric constant versus filler concentration at 1 MHz frequency

Fig.4.11(a-d) shows the behavior of dielectric loss with frequency for pure and dispersed samples at room temperature. The loss factor ($\tan\delta$) shows strong frequency dependence and decreases exponentially as frequency increases. The positive value of $\tan\delta$ indicates the dominance of inductive behavior. It is noticed that dielectric loss increases on increasing the concentration of filler and also with the fluence [14,15].

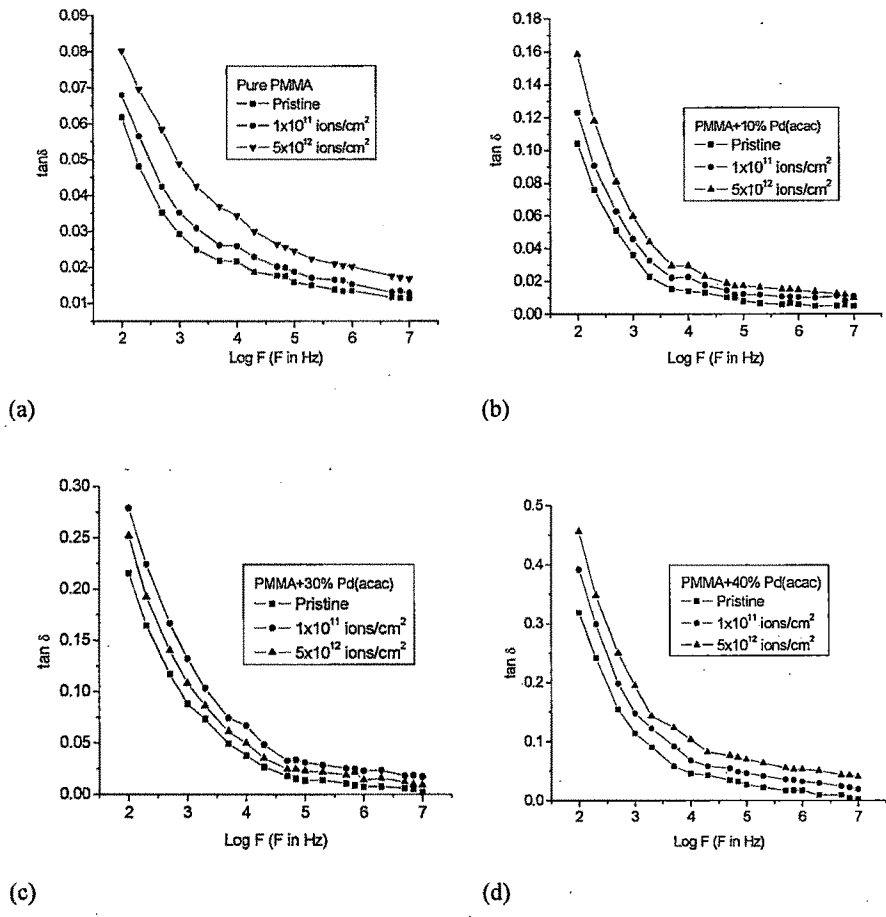


Fig. 4.11 dielectric loss ($\tan\delta$) versus log frequency of (a) Pure PMMA, (b) PMMA+10% Pd(acac), (c) PMMA+30% Pd(acac), (d) PMMA+40% Pd(acac) films

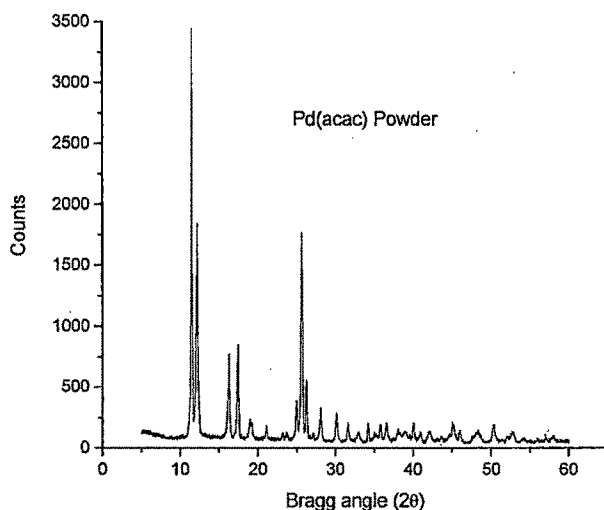
4.2.2 X-ray diffraction

Figure 4.12 (a) shows the XRD spectrum of organometallic compound. Fig. 4.12 (b-d) represents the diffraction patterns of the pristine and irradiated samples for the most prominent peaks. The peaks are obtained at $2\theta = 12.1^\circ$, 17.5° and 25.6° . The nature of the peak indicates the semi-crystalline nature of the sample. In both the cases of pristine and irradiated samples, the peaks obtained at the same position but with the different intensity. The crystallite size was calculated before and after the irradiation using Scherrer's equation [30] as discussed in section 2.3.3 of Chapter-2.

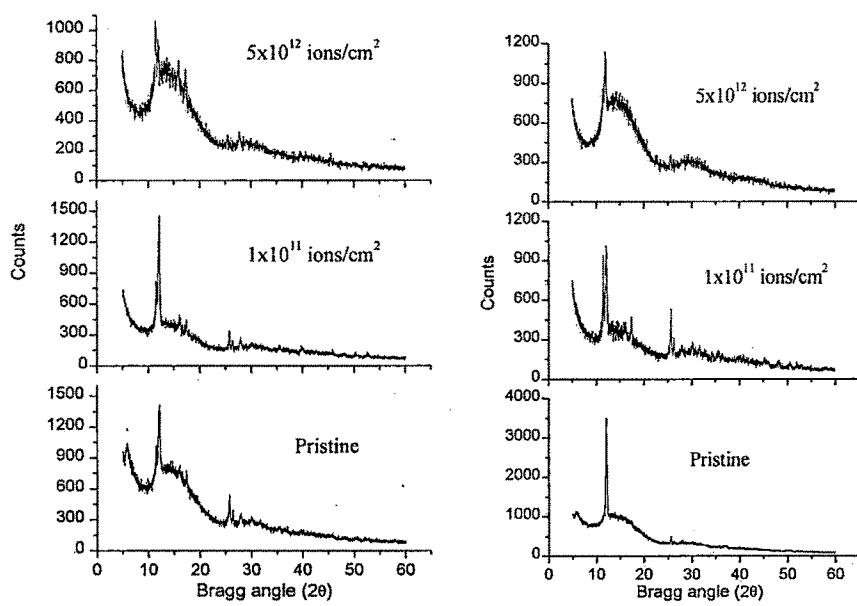
$$D = \frac{K\lambda}{l \cos \theta}$$

where K is constant approximately equal to unity and related to the crystalline shape, l is FWHM of the diffraction peak, D is crystalline size and θ is the angle between the atomic plane and both the incident and reflected beams.

The crystallite size obtained using above equation is listed in Table 4.1.

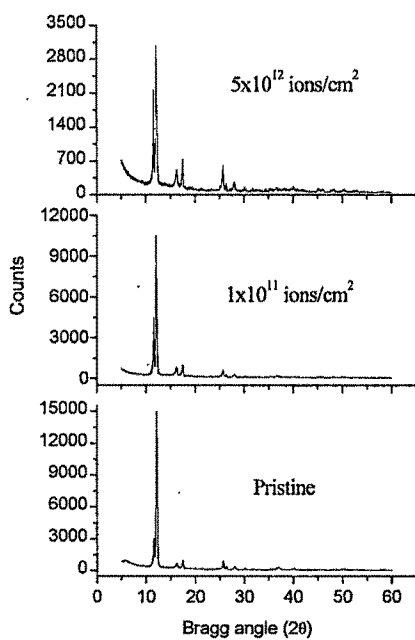


(a)



(b)

(c)



(d)

Fig. 4.12 XRD spectrum of (a) Pd(acac) powder, Pristine and irradiated composites of (b) PMMA+10% Pd(acac), (c) PMMA+30% Pd(acac) and (d) PMMA+40% Pd(acac)

Table 4.1 Crystalline Size and % crystallinity measurement

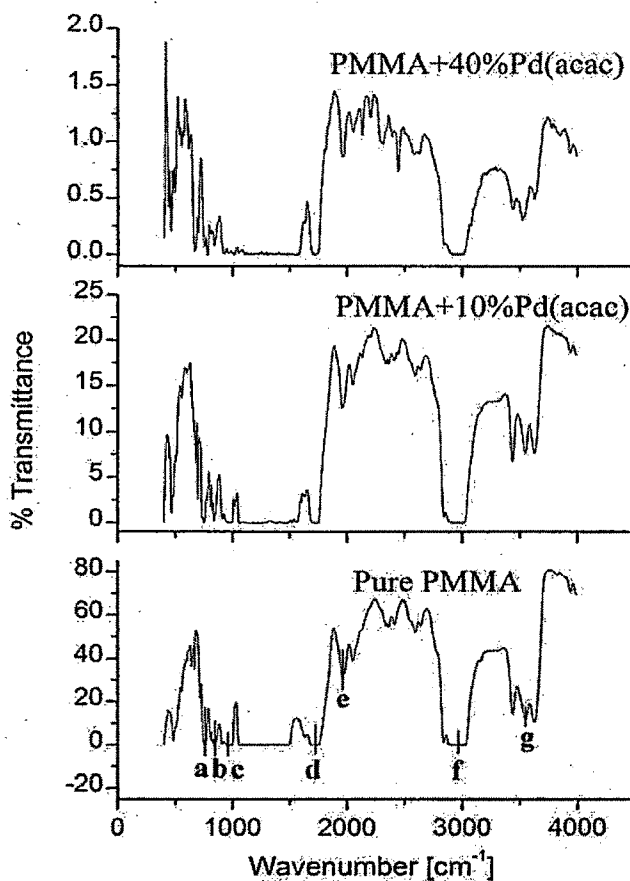
Sample	Crystalline size (nm)			% Crystallinity		
	Pristine	1×10^{11} ions/cm ²	5×10^{12} ion/cm ²	Pristine	1×10^{11} ions/cm ²	5×10^{12} ion/cm ²
PMMA+10 %Pd(acac)	6.6	5	4.9	10.2	8.8	7.5
PMMA+30 %Pd(acac)	22.7	18.1	16.2	17.3	14	12.3
PMMA+40 %Pd(acac)	23.4	23.3	21.4	38.8	34.5	21.5

Results show that crystallite size of the filler decreases slightly after irradiation. It is also observed that the intensity of the peak decreases upon irradiation and no significant change in the peak position is observed. This reveals that the lattice parameters do not change significantly. The decrease in intensity and broadening of the peak after irradiation indicates a decrease in crystallinity. The broadening of peak suggests an evolution of the polymer towards a more disordered state. Crystallite size also changes due to irradiation [31, 32].

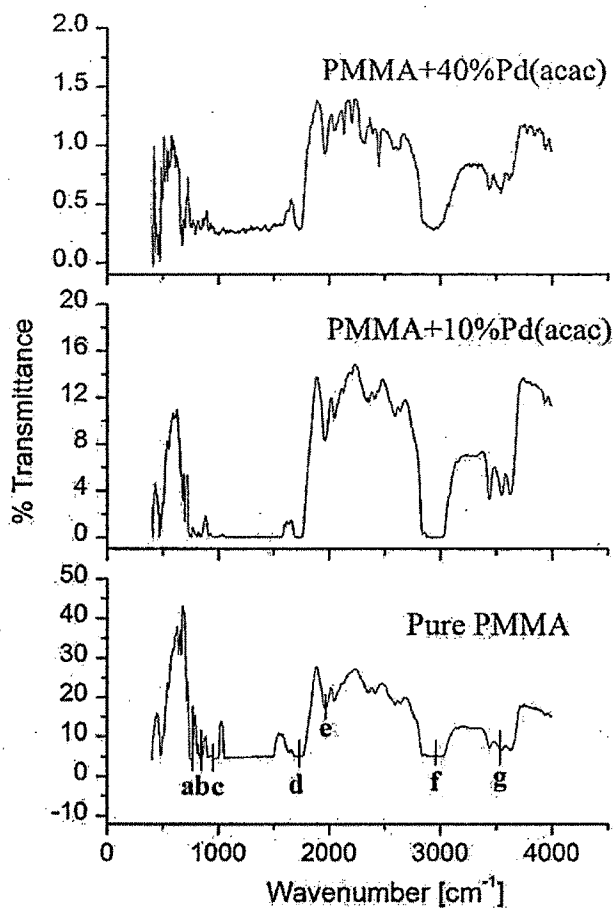
4.2.3 FTIR analysis

FTIR spectra of pristine and irradiated films of pure PMMA and (10, 30, 40%) Pd(acac) doped PMMA films have been studied and plotted in Fig. 4.13 (a, b). The absorption bands obtained from the spectrum of pure PMMA pristine are identified as (a) CH₂ rocking vibration (751 cm⁻¹), (b) CH₃ rocking (847 cm⁻¹), (c) C-O stretching vibration (990-1270 cm⁻¹), (d) C=O stretching vibration (1600-1800 cm⁻¹) (e) C=C stretching vibration (1920-2100 cm⁻¹) (f) C-H stretching vibration of CH₂ and CH₃ (2820–3080 cm⁻¹) (g) OH free stretching vibration (3400- 3600 cm⁻¹) [26]. The

C-O and C=O groups show a strong absorption in the range (990-1200 cm^{-1}) and (1600-1800 cm^{-1}) respectively depending on the immediate environment of these groups (Fig.4.13a). However, after irradiation, the peak intensities of functional groups are reduced due to emission of hydrogen and/or other volatile gases (Fig. 4.13b). This may be attributed to the breakage of chemical bonds and formation of free radicals, unsaturation, etc.



(a)



(b)

Fig. 4.13 FTIR spectrum for (a) Pristine and (b) Irradiated (5×10^{12} ions/cm²) composites

4.2.4 Scanning Electron Microscopy

The surface morphology of the pristine and irradiated films has been studied using SEM and shown in Figure 4.14(a-f) at 1 kX magnification. The surface roughness is observed to increase with concentration of filler and also with irradiation. The increase in roughness with filler concentration may be due to the increase of density and size of metal particles on the surfaces of the films [27]. SHI irradiation of

polymer composites leads, in general, to an increase in surface roughness due to large sputtering effects.

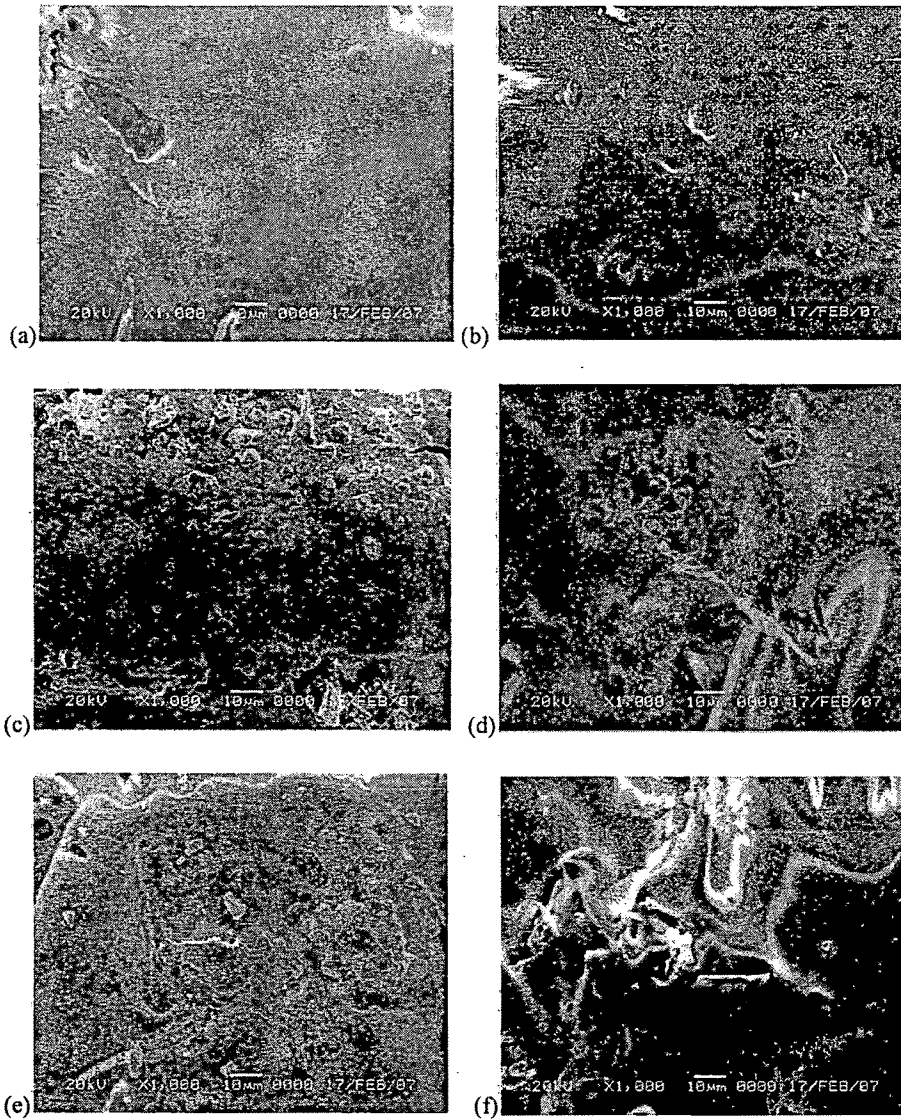


Fig. 4.14 SEM images of (a) Pure PMMA (pristine), (b) Pure PMMA (irradiated), (c) PMMA+10% Pd(acac) (pristine), (d)PMMA+10% Pd(acac) (irradiated), (e) PMMA+30%Pd(acac) (pristine) and (f) PMMA+30%Pd(acac)(irradiated) films

4.2.5 Optical Images

Optical images of pristine samples of pure PMMA and composite films were taken and shown in Fig. 4.15(a-c). The result shows that the roughness increases with increasing filler concentration, which is also corroborated with SEM results.

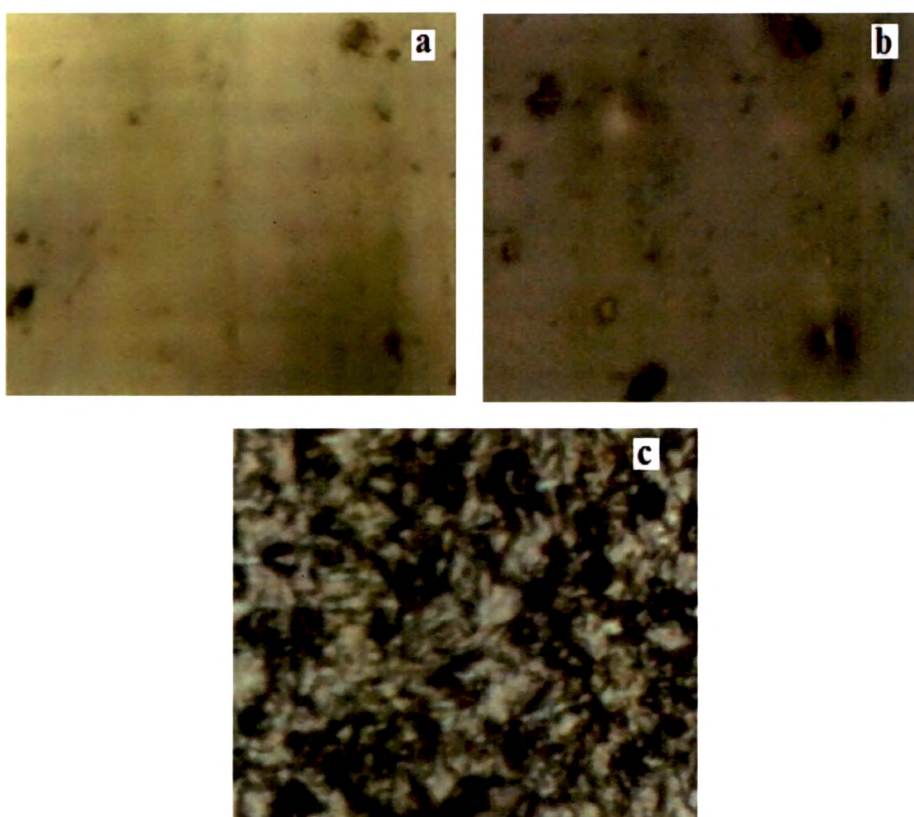


Fig. 4.15 Optical images of pristine films (a) Pure PMMA (b) PMMA+10% Pd(acac) and (c) PMMA+30% Pd(acac)

4.2.6 Differential scanning calorimetry

Fig. 4.16 shows DSC thermograms of pristine PMMA, pristine and irradiated (5×10^{12} ions/cm²) PMMA+40%Pd(acac) samples. The result reveals that the glass transition temperature (T_g) increases for the composite than the pure polymer but decreases

after irradiation. Glass transition temperature is characteristic of a material and represents the transition from amorphous glassy state to rubbery state. The increase in T_g of composites may be due to interactions of Pd(acac) and PMMA in more ordered state [32]. After irradiation T_g decreases, which reveals the amorphization of the composite after irradiation and it is also corroborated with XRD results.

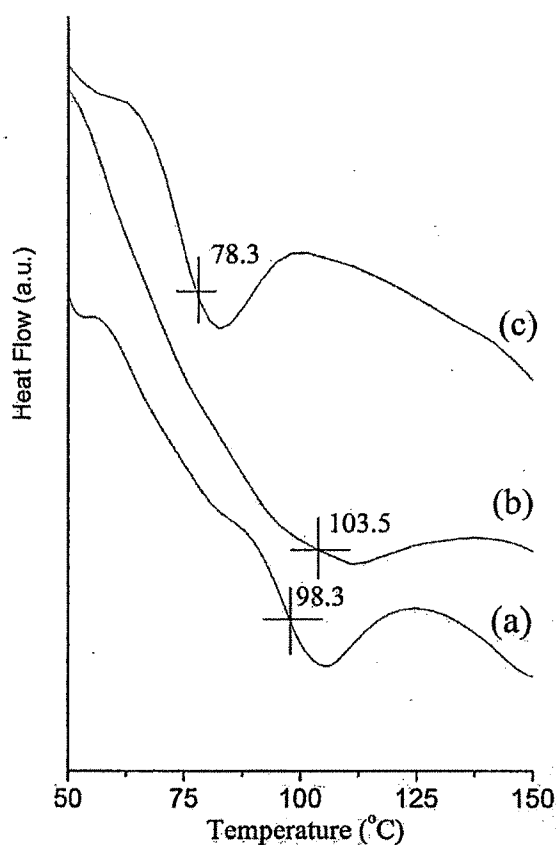


Fig. 4.16 DSC thermograms of (a) Pure PMMA (pristine) and (b) PMMA+40% Pd (acac)(pristine) and (c) PMMA+40% Pd (acac) (irradiated)

4.2.7 Conclusions

Dispersion of organometallic compound (Pd(acac)) in PMMA films enhanced the dielectric properties of pure polymer significantly. This may be attributed to the conductive phase formed due to dispersion of organometallic compound in polymer

matrix. Ion irradiation has further enhanced the dielectric properties. It may be attributed to the metal to polymer adhesion and conversion of the polymeric structure into a hydrogen depleted carbon network. An XRD analysis reveals that the crystalline size of the organometallic compound has decreased after ion beam irradiation. This may be due to deposition of large amount of energy and resulted in splitting/melting of nanometric grain. Crystallinity of the composites decreases due to chain scissioning with the ion fluence which induces amorphization. FTIR results also support the XRD analysis. The peak intensity of various functional groups is observed to decrease after irradiation. SEM/optical images reveal that the surface roughness increases with increasing the filler concentration as well as with ion fluence. Glass transition temperature (T_g) of pristine and irradiated samples was studied by using DSC analysis and it reveals that T_g decreases after irradiation and system moves towards disordered state due to interaction of SHI with material.

4.3 Effect of SHI (120 MeV Ni¹⁰⁺) on PMMA+Ni composites

4.3.1 AC electrical properties

(i) AC electrical Conductivity

The ac conductivities of the pristine and irradiated composites as a function of the frequency and concentration of the filler are shown in Fig. 4.17(a, b). It was calculated using equation 2.3.13 as explained in Chapter-2. The ac conductivity of the composites increases with increasing frequency and filler concentration (Fig.4.17(c)).

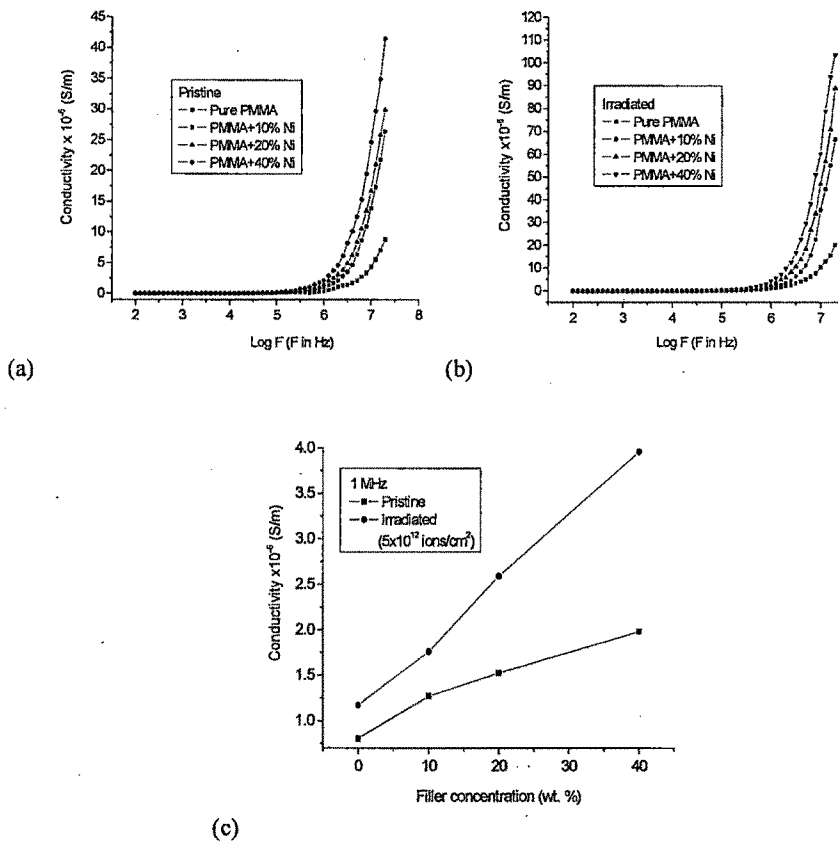


Fig. 4.17 AC conductivity versus log frequency for (a) Pristine and (b) Irradiated composite films, (c) AC conductivity versus filler concentration at 1 MHz frequency.

It is assumed that an electrical conducting path and network of connections could be formed in the composites with increasing the content of the filler. It is known that electrical conductivity of such composites depends on the type and concentration of the fillers [11, 12].

Irradiation is expected to promote the metal to polymer bonding and convert the polymeric structure into a hydrogen depleted carbon network, which makes polymer more conductive [13].

(ii) Dielectric property

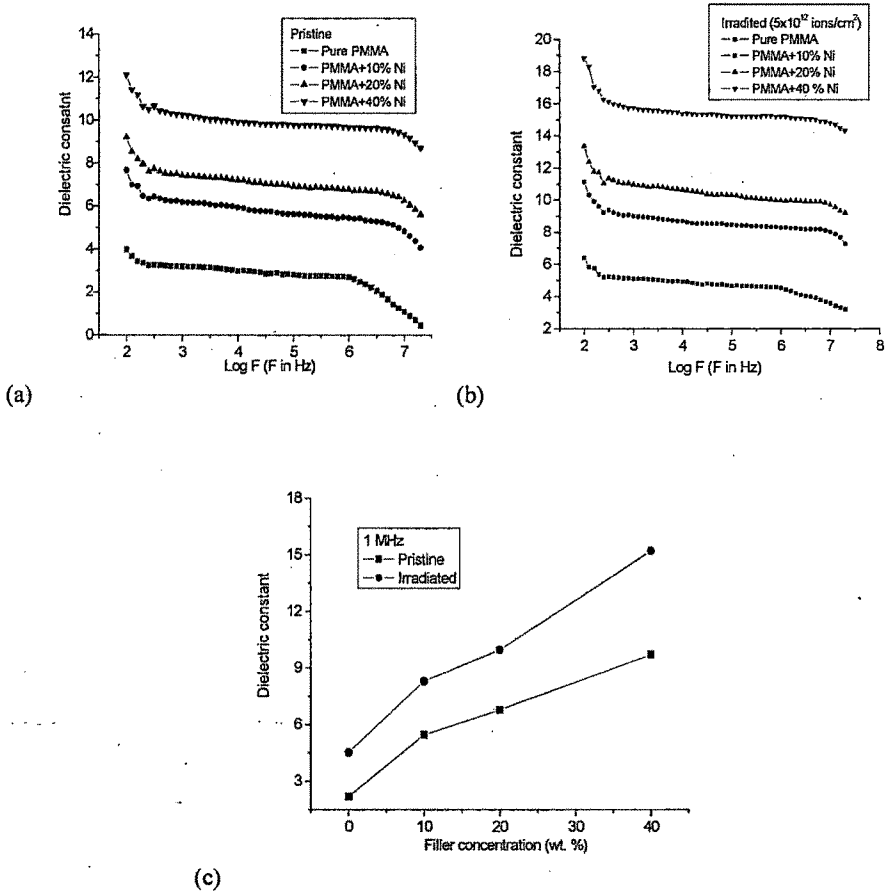


Fig. 4.18 Dielectric constant versus log frequency for (a) Pristine and (b) Irradiated samples (c) Dielectric constant versus concentration of filler at 1 MHz frequency.

Fig.4.18 (a, b) shows the variation of dielectric constant of pristine and irradiated composites as a function of frequency and calculated using equation 2.3.15 (Chapter-2).

At very high frequencies, the dipoles do not have time to align before the field changes its direction and so the dielectric constant is lower. The variation of dielectric constant as a function of concentration for pristine and irradiated Ni/PMMA composites at 1 MHz is shown in Fig.4.18(c). A significant increase in dielectric constant is observed with filler concentration. The increase in the dielectric constant with filler content is a direct consequence of interfacial polarization effect [19, 20] between polymer and the filler particles.

The dielectric constant of the composites is also a function of its capacitance, which is proportional to the quantity of charge stored on either surface of the sample under an applied electric field [21, 22]. In PMMA composite-filled with conducting fillers, the quantity of the accumulated charges will increase because of the polarization of the PMMA/filler at interfaces. The polarization makes an additional contribution to the charge quantity. From this point of view the dielectric constant of the composites will be higher than that of the pure polymer and it will also increase with increasing the filler content. The experimental result in Fig. 4.18 (a) supports this explanation. Therefore, the materials with high dielectric constant could be prepared by adding the conducting fillers. As evident from Fig. 4.18, the dielectric constant remains almost constant up to 100 kHz. At these frequencies, the motion of the free charge carriers is constant and so the dielectric constant presumably remains unchanged. As frequencies increases further, the charge carriers migrate through the dielectric and get trapped against a defect sites and induced an opposite charge in its vicinity. At these frequencies, the polarization of trapped and bound charges cannot take place and

hence the dielectric constant decreases [33]. It is also observed that dielectric constant increases for irradiated films. The increase in dielectric constant may be attributed to the chain scission and as a result the increase in the number of free radicals, unsaturation, etc.

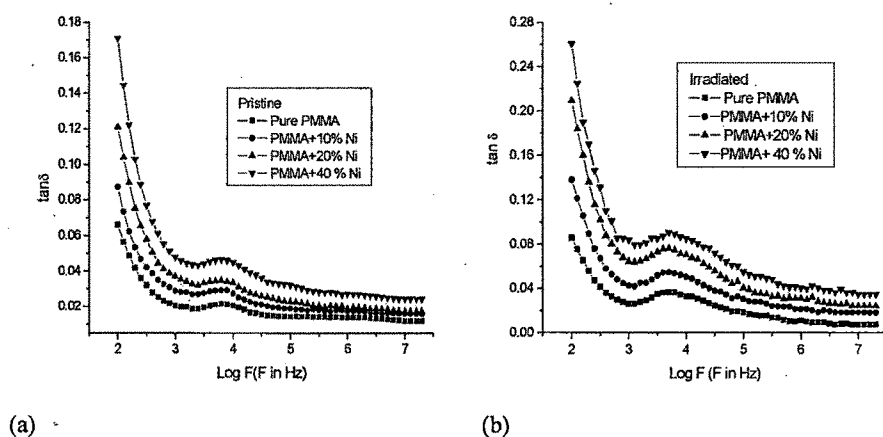
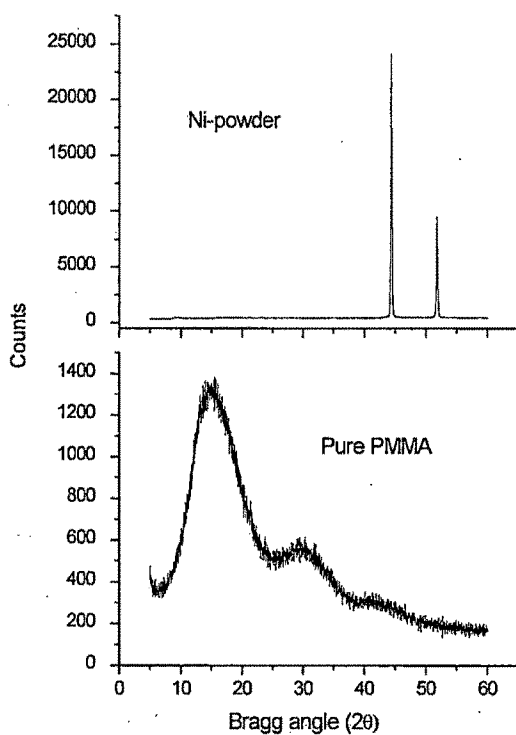


Fig. 4.19 Dielectric loss versus log frequency for (a) Pristine and (b) Irradiated (5×10^{12} ions/cm²) films

Fig. 4.19 (a, b) shows the frequency dependence of the dielectric loss for the pristine and irradiated Ni-PMMA composites. The dielectric loss decreases first then became less dependent on frequency. This is because the induced charges gradually fail to follow the reversing field causing a reduction in the electronic oscillations as the frequency is increased. The increase in dielectric loss with increasing filler contents may be attributed to the interfacial polarization mechanism of the heterogeneous system. Further moderate increase in $\tan \delta$ occurs due to the irradiation.

4.3.2 X-ray diffraction

X-ray diffraction spectrum in Fig. 4.20(a) shows the amorphous nature of PMMA and the crystalline behaviour of Ni powder. The average particle size of the Ni powder was obtained 39.8 nm. From Fig. 4.20(b) and (c), the most prominent peaks are obtained at $2\theta \sim 51.9$ and 44.6 in all the cases.



(a)

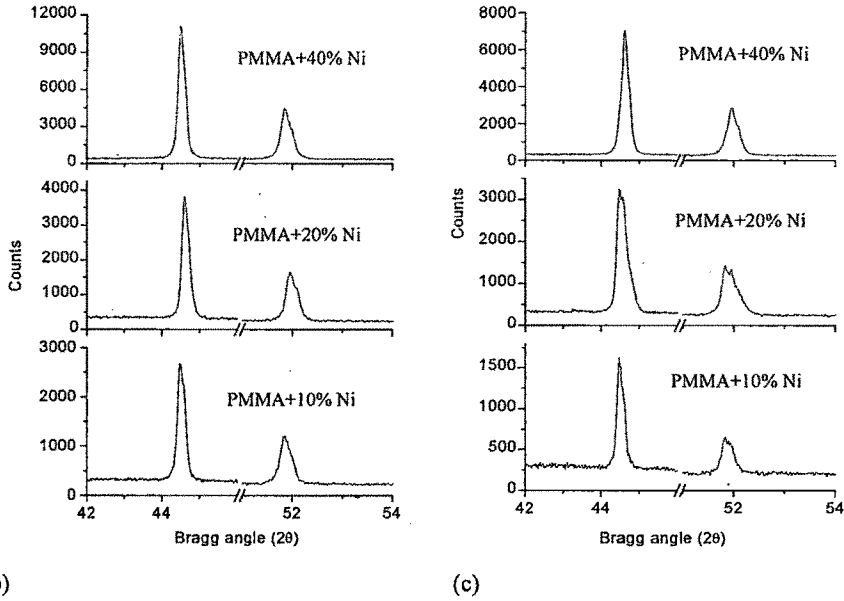


Fig. 4.20 XRD spectrum of (a) pure PMMA and filler (Ni -powder) (b) Pristine and (c) Irradiated (5×10^{12} ions/cm²) composites

The appearance of sharp peak in composite indicates some degree of crystallinity, although the decrease in intensity of the diffraction peak and slightly broadening of the peak after irradiation gives evidence of decrease in crystallinity. However no significant change in the peak position reveals that lattice parameters do not change significantly. The crystallite size has been calculated before and after irradiation using Scherrer's formula [30] as discussed in section of 2.3.3 of Chapter-2.

$$D = \frac{K\lambda}{l \cos \theta}$$

where K is constant approximately equal to unity and related to the crystalline shape, l is FWHM of the diffraction peak, D is crystalline size and θ is the angle between the atomic plane and both the incident and reflected beams.

Percentage crystallinity of the composites was determined by area ratio method. In this method the areas of amorphous and crystalline parts of the pattern were

calculated [34]. The average crystallite size and % crystallinity of the pristine and irradiated samples are listed in Table 4.2.

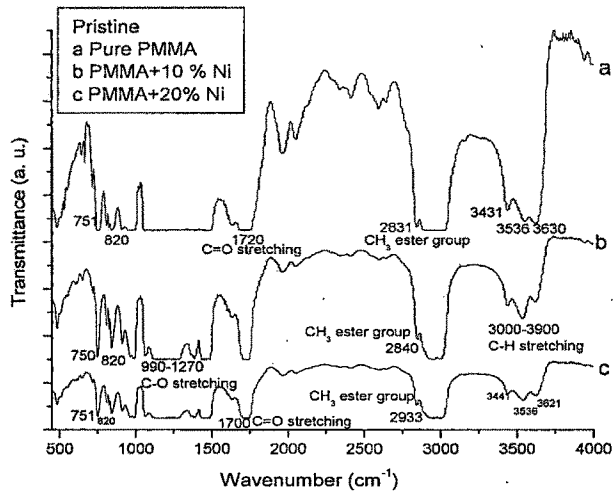
Table 4.2: Percentage crystallinity and crystalline size of the filler

Filler concentration (wt.%)	Average crystalline size (nm)		% Crystallinity	
	Pristine	5×10^{12} ions/cm ²	Pristine	5×10^{12} ions/cm ²
Ni powder	39.8	-	20.8	-
10	34.4	32.6	15.6	11.6
20	36.1	27.2	19.9	16.7
40	39.9	36.7	27.3	22.4

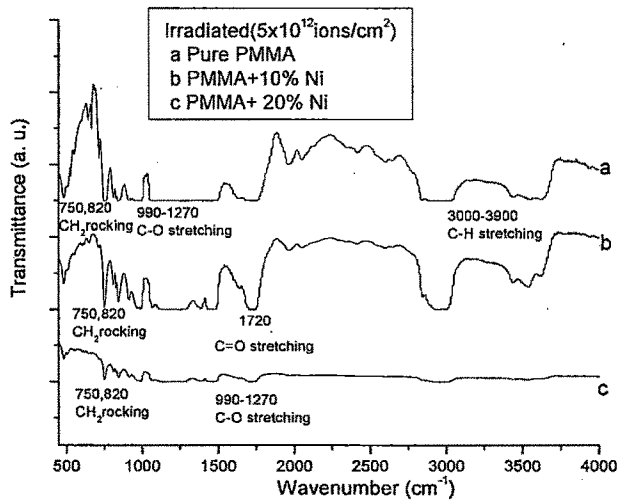
Irradiation induces large amount of energy deposition in the material and leads to decrease in crystallite size which may be attributed to splitting of crystalline grains. The chain scissioning due to irradiation (which is also corroborated with FTIR spectra) assumed to be responsible for the reduction in crystallinity of the composites.

4.3.3 FTIR analysis

Chemical response or the nature of chemical modifications can be studied by infrared spectroscopy. Fig. 4.21 (a, b) represents the FTIR spectra of the pristine and irradiated films (at fluence of 5×10^{12} ions/cm²) of Ni-PMMA composites at different concentrations.



(a)



(b)

Fig. 4.21 FTIR spectrum of (a) Pristine and (b) Irradiated composites

It shows the interactions between macromolecules and filler particles, the small shift and alteration of band shape are the result of changes in the nearest surrounding of functional groups. These observations are illustrated in Fig. 4.21 for bands in region 500-4000 cm^{-1} . For example, band at 2831 cm^{-1} in spectrum of pure PMMA occurs at

2840 cm^{-1} for PMMA+ 10% Ni and at 2933 cm^{-1} for PMMA+ 20% Ni. The band in the region 1000-1700 cm^{-1} , few new peaks are formed due to presence of filler, these peaks were not present in pure PMMA. Figure shows clearly the reduction in intensity of the peaks of irradiated samples as compared to pristine sample. At 1720 cm^{-1} , a peak is identified as C=O stretching vibrations in the pendant group (-COOCH₃) of PMMA. This peak decreases with the fluence of irradiation. An absorption band in the range of 1500-700 cm^{-1} comes from the C-O stretching vibration (1270-990 cm^{-1}), C-H bending vibration (1450-1350 cm^{-1}) and CH₂ rocking vibration (810 and 750 cm^{-1}) [26]. These peaks also decrease with the fluence. This shows that the C-O, C=O bonds and CH₂, CH₃ groups diminish with irradiation fluence. It is observed that polymer structure is converted in to hydrogen depleted carbon network.

4.3.4 Atomic force microscopy

The surface morphology of pristine and irradiated films of 10% and 40% Ni dispersed PMMA was studied by AFM on 5×5 μm^2 area as shown in Fig 4.22 (a-d).

Each AFM image was analyzed in terms of surface average roughness (Ra). The average roughness values obtained for unirradiated films are 0.7 nm (for PMMA+10% Ni) and 3.2 nm (for PMMA+40% Ni) and for corresponding irradiated films at the fluence of 5×10^{12} ions/ cm^2 , the roughness was obtained as 5.2 nm and 12.3 nm respectively. It is found that roughness increases as filler (Ni) concentration increases. The increase in roughness may be due to the increase of density and size of metal particles on the surfaces of the PMMA films [27]. Ion irradiation of polymers leads significant increase in surface roughness due to large sputtering effects, which is also corroborated with SEM results.

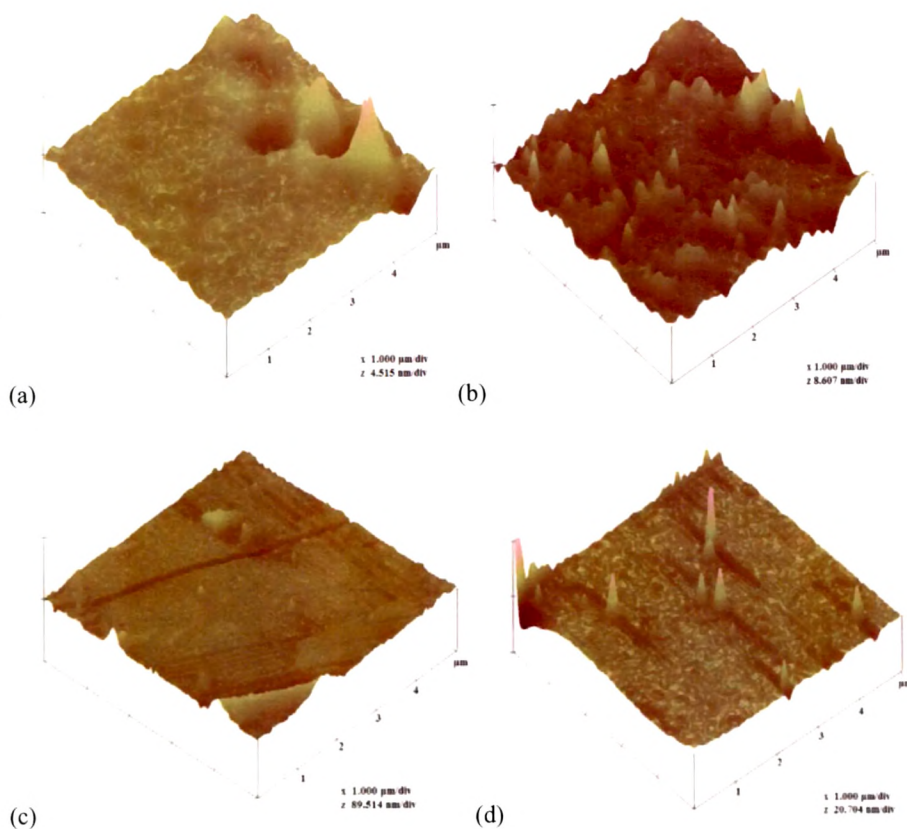


Fig. 4.22 AFM images for (a) PMMA+10% Ni (pristine), (b) PMMA+10% Ni (5×10^{12} ions/cm²) (c) PMMA+40% Ni (Pristine), (d) PMMA+40% Ni (5×10^{12} ions/cm²) films

4.3.5 Scanning electron microscopy

Fig. 4.23 (a-d) shows the SEM images of 10% and 40% Ni powder dispersed pristine and irradiated composite films with 1kX magnification.

After irradiation, significant change in surface morphology was observed. Considerable damage in the polymeric structure was observed after irradiation. Which is also responsible for decrease in crystallinity of the material as indicated in XRD analysis.

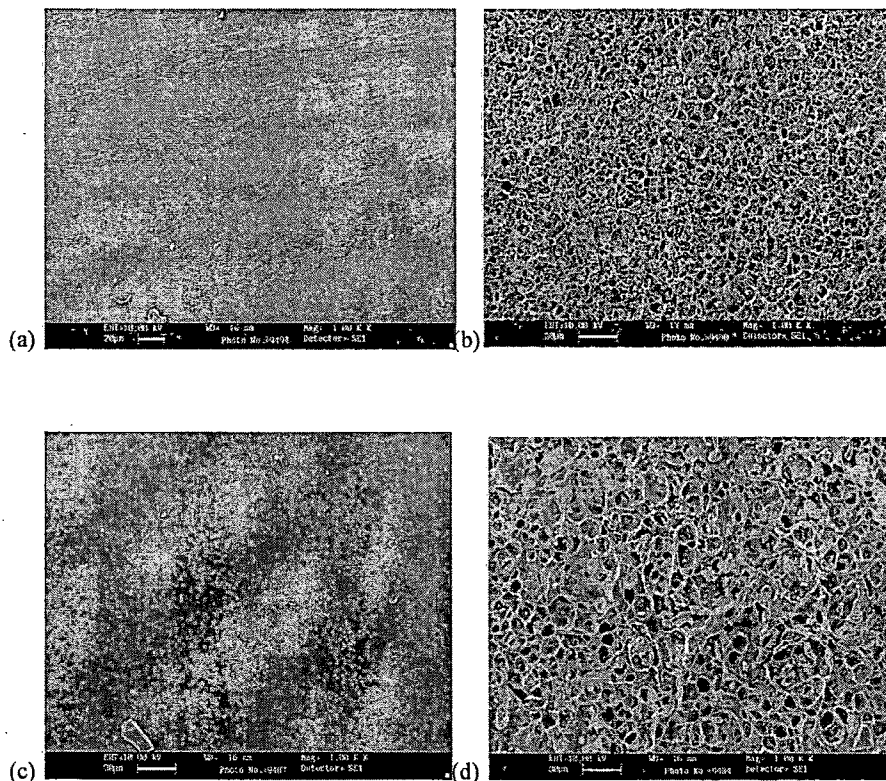


Fig. 4.23 SEM micrographs of (a) PMMA+10%Ni (pristine), (b) PMMA+10%Ni (irradiated), (c) PMMA+40% Ni (pristine) and (d) PMMA+40% Ni (irradiated) films

4.3.6 Conclusions

The dielectric properties of pristine and irradiated PMMA matrix composites filled with Ni conducting filler were studied over a broad range of frequency and concentration of filler. The conductivity of the composites increases with an increase in frequency and the content of the filler. Ion irradiation has been shown to significantly enhance dielectric properties of the composites. It may be attributed to (i) metal to polymer bonding and (ii) conversion of the polymeric structure into hydrogen depleted carbon network. Thus irradiation makes the polymer more conductive. The dielectric constant decreases slowly with increasing frequency. The dielectric loss also shows frequency dependent behaviour. It increases gradually with

a rise of the concentration of filler. This might be attributed to breakage of chemical bonds and resulting in the increase of free radicals, unsaturation etc as revealed from FTIR analysis. XRD results reveal that the crystalline size and percentage crystallinity decreases after irradiation. Surface properties were studied by AFM and SEM. The results show that average surface roughness increases due to irradiation, which may be attributed to a large sputtering effect due to SHI irradiation.

4.4 Effect of SHI (120 MeV Ni¹⁰⁺) on Polymer nanocomposites (PI+Fe)

For present work, thin films of polymer composites were prepared by RF co-sputtering of PI and Fe. Using RBS, concentration of Fe was found to be 0.5, 1 and 5%. The thickness of the films was studied using ellipsometry technique and obtained ~100 nm. These films were irradiated with 120 MeV Ni¹⁰⁺ ion beam at the fluence of 5×10^{12} ions/cm². Pristine and irradiated films were characterized by using AFM, MFM, UV-Vis spectroscopy and SQUID as explained in section 2.3 of Chapter-2. Results are presented in following sections.

4.4.1 AFM/MFM analysis

Purpose of this study is to throw light on the effect of SHI on surface topography and surface magnetic properties of thin film. MFM is used to provide information about the local magnetic structure. However, a precise comparison between height and phase images is required to separate true magnetic information from possible interference caused by the surface topography [35]. Imaging was performed with atomic force microscope operating in tapping/lift mode which combine interaction and constant height mode in order to separate short range topographic and long range magnetic signal [36-38]. Because Van der Waals forces only become significant for tip-sample distances < 10nm where as magnetic measurements can be alleviated by using large enough lift heights >17 nm.

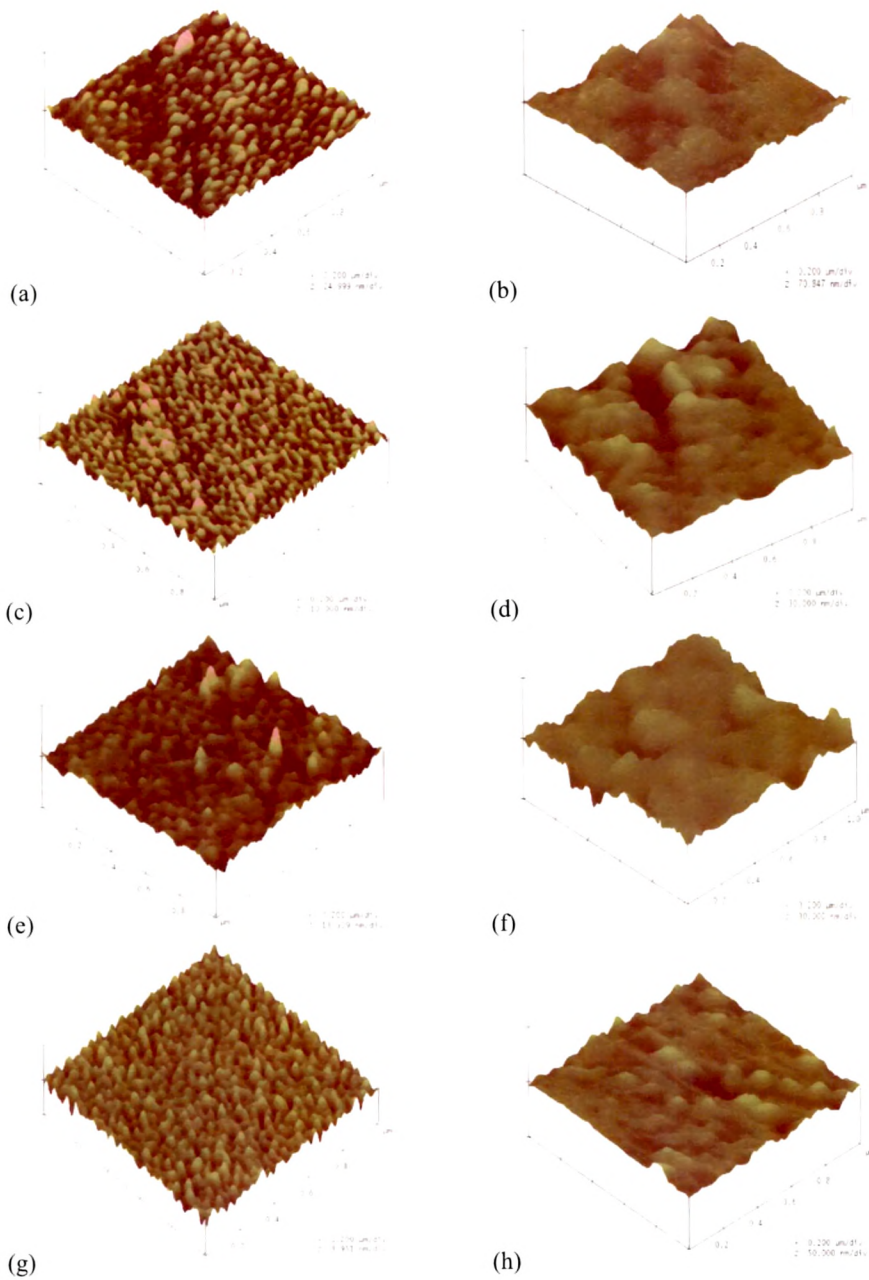
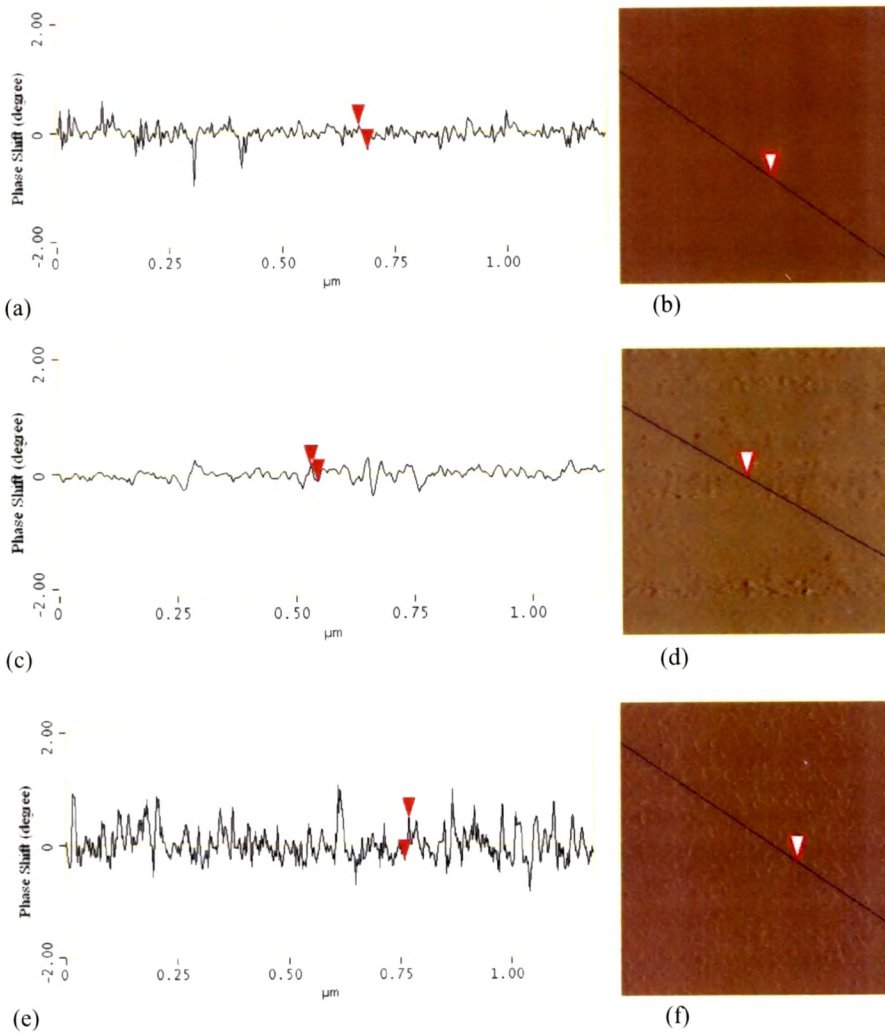


Fig. 4.24 AFM images of (a) Pure PI(pristine) (b) Pure PI (irradiated) (c) PI+0.5% Fe(pristine) (d) PI+0.5% Fe (irradiated) (e) PI+1% Fe (pristine) (f) PI+1% Fe (irradiated) (g) PI+5% Fe (pristine) (h) PI+5% Fe (irradiated) films

AFM images of films are shown in Fig.4.24(a,c,e,g) for pristine and Fig. 4.24 (b, d, f, h) for irradiated (5×10^{12} ions/cm²) samples. The average surface roughness of pristine

samples of pure PI, PI+0.5% Fe, PI+1% Fe and PI+5% Fe was obtained to be 0.9, 0.5, 0.8 and 0.8 nm respectively. The roughness value increases upon irradiation and found to be 4.0, 2.1, 4.4 and 2.3 nm respectively for the films. It reveals that the average surface roughness increases after irradiation. Irradiation induces large sputtering effect on the polymeric surface and this might be the cause of increase in surface roughness [10].



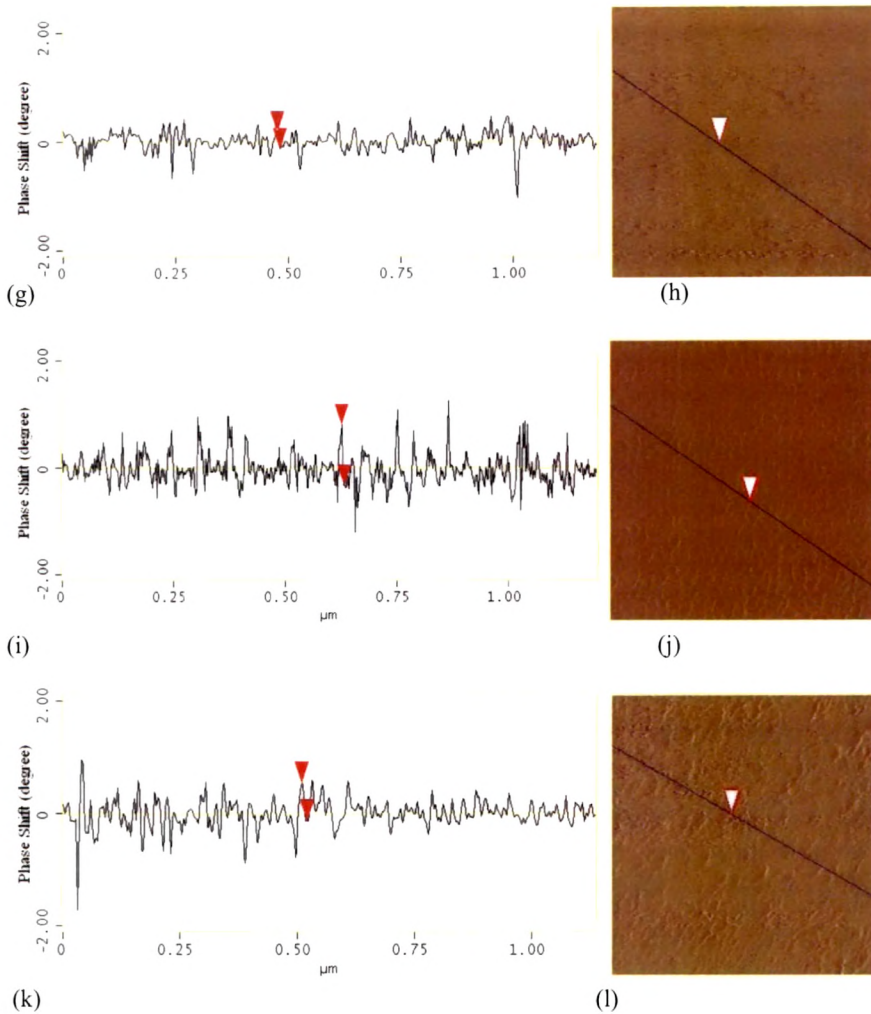


Fig. 4.25 (a,c,e,g,i,k) diagonal profile section magnetic force gradient and (b,d,f,h,j,l) Magnetic force gradient topographic images of pristine and irradiated PI+0.5%Fe, PI+1%Fe and PI+5%Fe composites respectively

It is observed from the figures that for low concentration of Fe, the magnetic contrast is not prominent but for 5% Fe, the images (j, l) of the films show magnetic ordering. Fig. 4.25 (a,c,e,g,i,k) shows line scan on one of the analysed areas giving an evidence that the magnetic signal is stronger for pristine (a,e,i) samples and decreases for irradiated (c,g,k) films. All the images were taken for $1 \times 1 \mu\text{m}^2$ area. These results are also confirmed by SQUID analysis.

4.4.2 SQUID

SQUID measurement of pristine and irradiated PMMA+5% Fe was done as shown in Fig. 4.26 and the obtained results are corroborated with MFM results and reveal that magnetization decreases after irradiation.

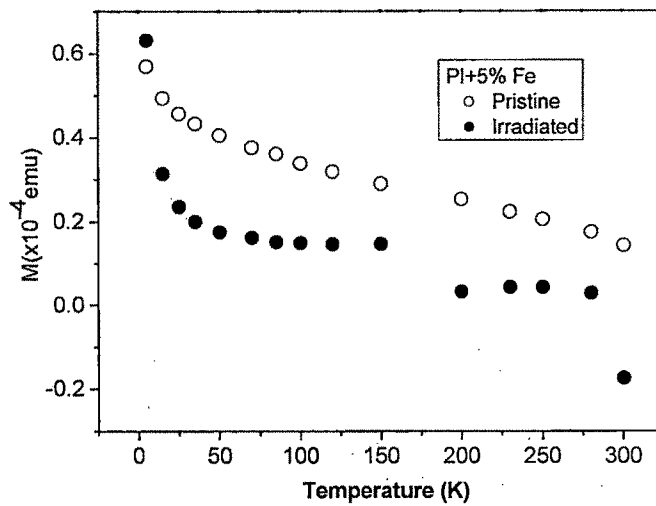


Fig. 4.26 SQUID analysis of pristine and irradiated PI+5% Fe films

4.4.3 UV-Vis Spectroscopy

Optical characteristic of the pristine and irradiated samples have been studied by means of UV-Vis Spectroscopy for the wavelength range of 250-900 nm. The optical band gap E_g is obtained by tauc's equation [39]

$$\text{i.e. } \omega \epsilon(\lambda) = (\hbar\omega - E_g)^2$$

Where $\epsilon(\lambda)$ is the optical absorbance and λ is the wavelength. The intersection of the extrapolated spectrum with the abscissa of the plot $\epsilon^{1/2}/\lambda$ versus $1/\lambda$ yields the band

gap. Calculated optical band gap is plotted as a function of filler concentration in Fig.

4.27.

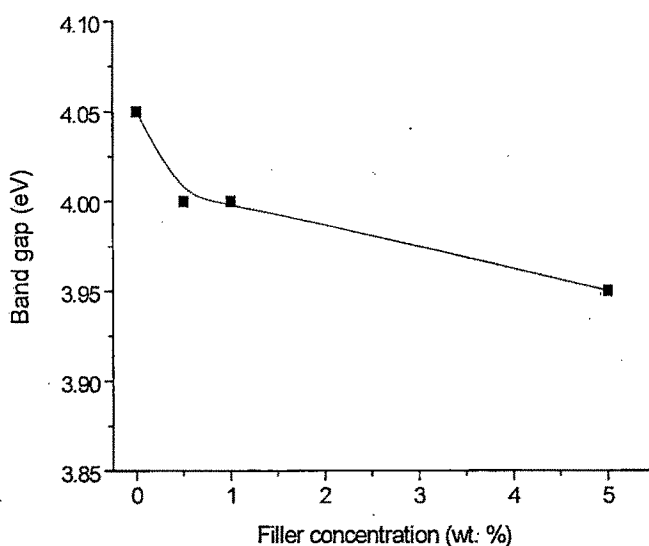


Fig. 4.27 Variation in band gap energy with filler concentration

Thus, the optical absorption method was used for providing information about the band gap energy of the composite material. It is observed that the band gap decreases with increasing the metal concentration. No significant change in band gap energy was observed after irradiation.

4.4.4 Conclusions

Metal doping enhances the optical properties of the polymer and makes it more conductive. Magnetization increases with metal concentration. Irradiation of such films with heavy ion beam increases the roughness of the material and reduces the magnetization. No appreciable change in the optical band gap was obtained after irradiation as revealed from UV-Vis analysis.

4.5 Summary

Three different composites have been studied using 120 MeV Ni^{10+} beam irradiation. AC electrical, mechanical, structural, thermal and surface properties have been studied using different characterization techniques.

AC electrical conductivity of all pristine and irradiated composites at 10% filler concentration is shown in Fig. 4.28.

Conductivity is observed to increase after irradiation in each case. It is assumed that an electrical conducting path and network of connections could be formed in the composites with increasing the content of the filler. It is known that electrical conductivity of such composites depends on the type and concentration of the fillers. Irradiation is expected to promote the metal to polymer bonding and convert the polymeric structure into a hydrogen depleted carbon network, which makes polymers more conductive.

Figure 4.28 shows comparison of conductivity of all composites before and after irradiation. For the sake of comparison filler fraction (10%), fluence of Ni^{10+} beam (5×10^{12} ions/cm²) and frequency (10 MHz) have been considered constant. Similar nature of the graphs was obtained for all composites with different filler particles. The magnitude of the dielectric constant varies with filler specie.

Similar study for dielectric constant of all composites have been done and shown in Fig. 4.29. It is observed that dielectric constant increases after irradiation. Dielectric loss was studied for all pristine and irradiated composites and results show frequency and fluence dependent behaviour. In all cases, it reveals that dielectric loss is positive and signifies inductive behaviour of the material.

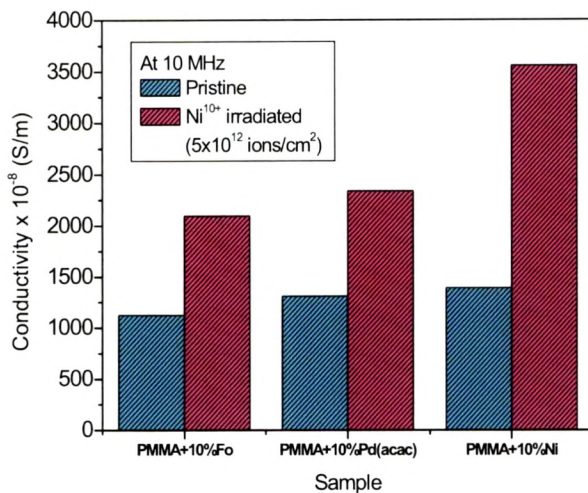


Fig. 4.28 Comparison of conductivity of pristine and irradiated (fluence of 5×10^{12} ions/cm²) composites at 10 MHz

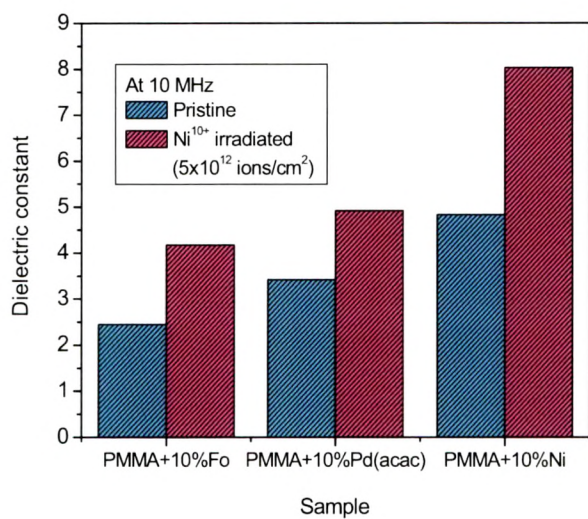


Figure 4.29 Comparison of dielectric constant of pristine and irradiated (fluence of 5×10^{12} ions/cm²) composites at 10 MHz

XRD of pristine and irradiated samples of PMMA+Pd(acac)/Ni have been studied and the results reveal that the crystalline size and %crystallinity of the sample

decreases upon irradiation. SHI induces large amount of energy deposition in the material which leads to decrease in crystallite size and % crystallinity due to splitting of crystalline grains and improved disorderness in the composites respectively.

FTIR analysis shows small shift and alteration in the peak position due to changes in the nearest surrounding of functional groups because of the presence of filler particles. The reduction in peak intensities after irradiation is attributed to the breakage of few chemical bonds and formation of free radicals, unsaturation, etc. due to emission of hydrogen and/or other volatile gases.

AFM study reveals that the average surface roughness increases after irradiation in all cases. This might be attributed to large sputtering effect due to high energy ion interaction with composite surface.

Thermal analysis was carried out by means of DSC. The result reveals that the glass transition temperature (T_g) shifted towards higher temperature for the composite in comparison to the pure polymer but decreases after irradiation. After irradiation T_g decreases, which reveals the amorphization of the composite after irradiation and it is also corroborated with XRD results.

Thin film was prepared by RF co-sputtering of Fe and PI on Si and glass substrate with the thickness of ~100 nm. SHI effect on the magnetic, optical properties and surface morphology of the films was carried out. Magnetic properties of the films are observed to degrade upon irradiation as revealed from MFM and SQUID measurement. Average surface roughness of the thin film increases upon SHI interaction. UV-Vis spectroscopy reveals that the optical band gap decrease with increase in metal concentration. No significant change in band gap energy was observed due to irradiation.

References

- [1] F. C. Schilling, A. E. Tonelli and A. L. Cholli, *J. Poly. Sci.* 30 (1992) 91.
- [2] R. Mehnert *Nucl. Instrum. Meth. B* 105 (1995) 348
- [3] A. Elwy, M. M. Badawy and G. M. Nasr *J. Poly. Degrad and Stability* 53 (1996) 289
- [4] E. H. Lee, G.R. Rao, L.K. Mansur. *Mater Sci Forum* 248–249 (1997) 135.
- [5] H.B.Luck, *Nucl. Instr. & Meth. B.* 202 (1982) 497.
- [6] V.N. Popok, V.B.Odzhaev, I.P.Kozlov, I.P.Kozlov, I.I. Azarko, I.A. Karpovich, D.V.Sviridov, *Nucl. Instr. & Meth. B* 129 (1997) 60.
- [7] N.L.Singh, Sejal Shah, Anjum Qureshi, F. Singh, D.K.Avasthi, V.Shrinet, V.Ganesan *Poly. Degrad. Stab.* 93 (2008) 1088.
- [8] N.L.Singh, Sejal Shah, Anjum Qureshi, P. K. Kulariya, D. K. Avasthi, A. M. Awasthi. *Rad. Eff. and Def. in Solids* 164 (10) (2009) 619.
- [9] N.L.Singh, Sejal Shah, Anjum Qureshi, A.Tripathi, F.Singh, D.K.Avasthi, P.M.Raole, *Bull of Mat. Sci.* (Communicated).
- [10] Sejal Shah, N. L. Singh, V. Shivakumar, Indra Sulania, A. Tripathi, F. Singh, D. K. Avasthi, R. V. Upadhyay *Int. Conf. on Electrolyte ceramics (ICE-2009)* Dec 13-17 2009, New Delhi, communicated.
- [11] M. Abu-Abdeen, G.M. Nasr, H.M. Osman, A.I. Abound. *Egypt J Sol.* 25 (2002) 275.
- [12] Y. P. Mamunya, V.V. Davydenko, P. Pissis, E. V. Lebedev. *Eur Poly J.* 38(2002)1887.
- [13] Y.Q.Wang, M. Curry, E. Tavenner, N. Dobson, R.E. Giedd. *Nucl Instrum Meth. B* 219-220 (2004) 798.

- [14] N.L.Singh, Anita Sharma, D.K.Avasthi, M.S.Gadkari, V.Shrinet. *Rad. Effects and Defects in Solids* 160 (2005) 99.
- [15] N. L. Singh, Anjum Qureshi, F.Singh, D. K. Avasthi. *Mat. Sci. & Eng. B* 137 (2007) 85.
- [16] A.K. Jonscher. *Phys Status Solidi B* 83 (1977) 585.
- [17] Anjum Qureshi, Sejal Shah, N.L.Singh, F.Singh, D.K.Avasthi. *J. Macromolecul A* 45 (2008) 265.
- [18] A.K. Jonscher. *Nature* 267(1977)673.
- [19] S. Ghany, A.E. Salam, G. M. Nasr. *J Appl Polym Sci.* 77 (2000) 1816.
- [20] S.H. Foulger. *J Appl Polym Sci.* 72(1999)1573.
- [21] Z. M. Dang, Y.H. Zhang, S-C. Tjong. *Synth Met* 146 (2004) 79.
- [22] D. Yu, J. Wu, L. Zhou, D. Xie, S.Wu. *Compos Sci Technol* 60 (2000) 499.
- [23] T. Phukan, D. Kanjilal, T.D. Goswami, H. L.Das. *Nucl Instr.Meth. B* 234 (2005) 520.
- [24] Anjum Qureshi, N.L.Singh, Keyur Somani, A.K.Rakshit, F.Singh, D.K.Avasthi. *Ind. J. Pure and Appl. Phys.*, 45 (2007) 57.
- [25] Anjum Qureshi, N.L.Singh, Sejal Shah, P. Kularia, F.Singh and D.K.Avasthi. *Nucl. Instr. & Meth. B* 266 (2008) 1775.
- [26] H.W.Choi, H.J.Woo, W.Hong, J.K.Kim, S.K.Lee, C.H.Eum. *Appl. Surf. Sci* 169 (2001) 433.
- [27] X. Yan, X. Tao, X. Shan, W. Xiaobo, Y. Shengrong. *Nanotechnology* 15(2004)1759.
- [28] A. Pelaiz-Barranco, *Scripta Materialia* 54 (2006) 47.
- [29] L.A. Dissado, R. M. Hill, *Proc. Roy. Soc. London* 390 (1983) 131.
- [30] P. Scherrer, *Gott. Nachr* 2 (1918) 98.

- [31] H.S. Virk, P.S.Chandi and A.K. Srivastava, Bull. Mater. Sci. 24(5) (2001) 529.
- [32] T.K. Vishnuvardhan, V.R. Kulkarni, C. Basavaraja, S.C. Raghavendra, Bull. Mater. Sci. 29(1) (2006) 77.
- [33] A. K. Jonscher, Dielectric relaxation in solids. London: Chesla dielectric press;1983.
- [34] Serap Kaviak, Hatice Kaplan Can, Ali Guner, Zakir Rzaev, J. Appl.Poly. Sci. 90 (2003) 1708.
- [35] S.A Koch, R. H. te Velde, G. Palasantzas and J. Th. M. De Hosson, Appl. Phy. Letters 84 (2004) 556.
- [36] S. Porthun, L. Abelmann and C. Lodder, J. Magn. Magn. Mater, 182 (1998) 238.
- [37] P. Grutter, H. J. Mamin, D. Ruger, Scanning Tunneling Microscopy II, edited by R. Wiesendanger and H. J. Guntherodt (Springer, Berlin 1992), P 151.
- [38] F. Singh, D. K. Avasthi, O. Angelov, P. Berthet, J.C. Pivin Nucl. Instrum. Meth B 245 (2006) 214-218.
- [39] A. Das, S. Dhara, A. Patnaik, Physical Rev. B, 59 (1999) 11069.